Structural and functional damage to neuronal nuclei caused by extracellular tau oligomers

Xuehan Sun
Beijing, China

B.S., University of California, San Diego, 2017

A Dissertation presented to the Graduate Faculty of the University of Virginia in Candidacy for the Degree of Doctor of Philosophy

Department of Biology

University of Virginia
May 2023

Abstract

Neuronal nuclei are normally spherical with a smoothly contoured surface. However, in Alzheimer's disease (AD) and other tauopathies, neuronal nuclei often develop deep invaginations including the nuclear lamina. The lamina, a meshwork of intermediate filaments on the inner face of the inner nuclear membrane, plays crucial a role in various nuclear activities, such as chromatin organization, nucleocytoplasmic trafficking of macromolecules, cell cycle regulation, and apoptosis. Previous research has shown that invaginated neuronal nuclei are found in human AD brain. In Drosophila melanogaster neurons*, in vivo* expression of pathogenically mutated human tau also causes nuclear lamina invagination [1]. In light of this background, we aimed to investigate the impact of pathological nuclear invagination in mammalian neurons.

The data presented in this dissertation demonstrate that lamina invagination is a feature of AD and related tauopathies *in vivo*. Neurons in post-mortem human AD cortices have a high frequency of such invaginations, as do those from the deep cortical layers of mouse models featuring tau pathology (PS 19 and CVN). Furthermore, we discovered that extracellular tau oligomers (xcTauOs) trigger rapid and long-lasting lamina invagination in cultured mouse neurons. This response depends on intracellular tau, as nuclear invagination is not observed in neurons derived from tau knockout mice exposed to xcTauOs, unless they express human tau by lentiviral transduction. Moreover, exposure to xcTauOs results in defective nucleocytoplasmic transport, changes in chromatin organization and transcription profile.

Together, these data establish that nuclear invagination is common in both naturally occurring human AD and transgenic mouse models of AD. They also suggest

that xcTauOs are a likely trigger of this phenomenon through a mechanism that relies on intracellular tau, causing alterations in many critical cellular processes.

Acknowledgements

First, I would like to express my gratitude to my mentor, George Bloom. I'm grateful for the time and effort he put into my training. With his advice, guidance, and support, I felt empowered to explore my own scientific ideas over the course of my PhD. What he offered was invaluable to my career. I'm also thankful to current and former members of Bloom lab. The camaraderie of the group made me look forward to going into the lab every day. I would not forget those lively conversations we had while working at the bench. I thank Yu Shi and Subhi Saibaba, who helped me complete the histological analysis of human and mouse brain tissues.

I would then like to thank my thesis committee, Dr. Chris Deppmann, Dr. Thurl Harris, Dr. Xiaorong Liu, and Dr. John Lukens. They were always supportive and offered many constructive advice that helped me finished my thesis. Additionally, I would like to thank the department for being such a welcoming and friendly group. By sitting on the graduate committee, I recognized all the work Biology department has done for its graduate student and am thankful for that.

Lastly, I would like to thank my parents. I'm incredibly grateful for what they have been doing for me. It's a challenging reality to come to terms with, knowing that their daughter is always thousands of miles away. Yet they wholeheartedly support my endeavors in all these years. I would also like to thank all my friends. They are always there for me.

Table of Contents

List of Abbreviations

AβO	Amyloid-β oligomer
AD	Alzheimer's Disease
AIS	Axon initial segment
APP	Amyloid precursor protein
ARA	Arachidonic Acid
ARIA	Amyloid-related imaging abnormalities
ATF6	Activating transcription factor 6
ChIP-Seq	Chromatin immunoprecipitation sequencing
CSF	Cerebral spinal fluid
CTF	C-terminal fragment
ER	Endoplasmic reticulum
FDA	The United States Food and Drug Administration
FTD	Frontotemporal dementia
H3K9Me3	Trimethylated lysine 9 of histone 3
HAT	Histone acetylase
HDAC	Histone deacetylase
HMT	Histone methyltransferase
HSPG	Heparan sulfate proteoglycan
iPSC	Induced pluripotent stem cell
iN	Induced neurons
INM	Inner nuclear membrane
LAD	Lamina associated domain

LAP	Lamina associated peptide
LBR	Lamin B receptor
lincRNA	Long intergenic non-coding RNA
LRP1	Low-density lipoprotein receptor-related protein 1
MCI	Mild cognitive impairment
MTBR	Microtubule binding repeat
miRNA	microRNA
NE	Nuclear envelope
NES	Nuclear export sequence
NFT	Neurofibrillary tangles
NLS	Nuclear localization sequence
NMDA	N-methyl-D-aspartate
NPC	Nuclear pore complex
NUP	Nucleoporin
ONM	Outer nuclear membrane
PART	Primary age-related tauopathy
PCH	Pericentromeric heterochromatin
PCR	Polymerase chain reaction
PET	Positron emission tomography
PHF	Paired helical filaments
PSP	Progressive Supranuclear Palsy
PTM	Post-translational modifications
RanGAP	Ran GTPase activating protein

RanGEF	Ran guanine nucleotide exchange factor
RAP	Receptor-associated protein
RNA-seq	RNA sequencing
scRNA-seq	Single-cell RNA sequencing
scATAC-seq	Single-cell transposase-accessible chromatin sequencing
UPR	Unfolded protein response
vGlut1	Vesicular glutamate transporters 1
xcTauOs	Extracellular tau oligomers

Chapter 1

Introduction

Chapter 1. Introduction

Tau was first identified in 1975 as a microtubule-associated protein [2]. Despite being natively unfolded and having little tendency to aggregation, the insoluble aggregates containing tau, such as paired helical filaments (PHFs) and neurofibrillary tangles (NFT), characterize a class of neurodegenerative disorders known tauopathy, including but not limited to Alzheimer's Disease (AD), progressive supranuclear palsy (PSP), and some forms of frontotemporal dementia (FTD). Though researchers have made significant strides in this field, the connection between tau pathology and neuronal dysfunction and degeneration remains unclear.

1. Alzheimer's Disease

In 1906, Alois Alzheimer documented the case of Auguste Deter in his seminal article. The patient initially presented to the mental hospital exhibiting symptoms of disorientation, delusions, and paranoid thoughts. Over the course of five years, she progressed into memory impairment, apraxia of speech, and eventually lost all cognitive abilities. After the autopsy, Alzheimer examined her brain histologically and described the presence of neurofibrillary tangles and amyloid plaques, which are now recognized as the two hallmarks of the disease bearing his name. Today, AD is the most common type of dementia, accounting for about 60% to 80% of all cases. In 2022, it was estimated that 6.5 million Americans were living with AD and this number is projected to 13.8 million in 2060. AD, one of the leading causes of morbidity and mortality, incurs substantial economic and societal cost. The lifetime cost of care for individuals with dementia is more than twice that of individuals without. In 2022, the annual payment for care was

$321 billion and projection suggests a cost of just under $1 trillion in 2050 (in 2022 dollars) [3].

Strictly speaking, a definitive diagnosis of AD can only be confirmed by post-mortem histological evaluation, as the disease is defined by the presence of neurofibrillary tau tangles and amyloid plaques. However, it is now accepted that the pathophysiological changes underlying cognitive dysfunctions occur many years before symptoms become noticeable. This long preclinical stage provides a critical window for early therapeutic intervention, which requires timely and accurate diagnosis antemortem in the clinics. In 2011, Alzheimer's Association and the National Institute on Aging of the National Institutes of Health published updated criteria and guidelines for the diagnosis of AD. The current guideline recognizes that AD progresses along a continuum with three broad phases: preclinical AD, mild cognitive impairment (MCI) due to AD, and dementia due to AD, depending on the extent to which symptoms interfere with everyday activities. The core clinical criteria still focus on cognitive and behavioral impairments, but have expanded beyond amnesia and included other aspects of cognitive impairment, such as language production, reasoning, computation, and problem solving. These can be evaluated through a combination of cognitive assessment and history taken from the patient and knowledgeable informants [4].

The guideline also recognized the potential of biomarkers for research purposes, while acknowledging that further validation and standardization are required before applying biomarker evidence for clinical diagnosis. Biomarkers are measurable indicators of pathogenic processes. They can be broken into two classes based on the biology being measured: biomarkers that reflect the core components of AD (Aβ and tau) and those that

measure downstream neurodegeneration. The most widely investigated biomarkers of Aβ accumulation include low Aβ42 concentration in cerebrospinal fluid (CSF) and abnormal tracer retention on amyloid positron emission tomography (PET) imaging. Aβ42 is normally mobilized from the brain interstitial fluid into the CSF and blood, whereas it aggregates into oligomers and fibrils in the AD brain parenchymal, resulting in decreased CSF Aβ42 levels. The diagnostic accuracy can be improved by taking the ratio of aggregation prone Aβ42 to soluble Aβ40 (Aβ42/ Aβ40), which is highly concordant to amyloid PET [5]. Three radioactive tracers ([18F] florbetapir, [18F] flutemetamol, and [18F] florbetaben) that selectively bind to Aβ aggregates has been approved by US Food and Drug Administration (FDA) for PET imaging. Additionally, regional reduction of glucose metabolism is also characteristic in the AD brain. Decreased uptake of [(18)F] fluorodeoxyglucose on PET imaging has long been used clinically to detect functional changes in AD brains [6]. Given that CSF sampling requires an invasive spinal tap and PET imaging accompanies considerable radiation exposure, current research focuses on identifying plasma biomarkers in clinical practice. For example, several studies demonstrated that p-Tau181 and p-Tau217 are robust plasma biomarkers to detect early pathological changes related to AD [7-10].

FDA has approved seven drugs for the treatment of AD. Five of them (donepezil, rivastigmine, galantamine, memantine, and memantine combined) are prescribed for moderate and severe cases. While these drugs can temporarily ameliorate symptoms, they do not stop disease progression. Memantine, a non-competitive N-methyl-D-aspartate (NMDA) receptor antagonist, works by blocking the pathological sustained, elevated cation flow through NMDA channel, which otherwise may be excitatory toxic to neurons.

On the other hand, the other three drugs are cholinesterase inhibitors that increase the availability of acetylcholine at the synaptic cleft. Enhancing cholinergic neurotransmission may improve cognitive functions in the short term and delay the onset of more severe symptoms. These drugs are generally well-tolerated, with mild side effects.

The FDA's approval of aducanumab in June 2021 marked a significant, though controversial, milestone in the treatment of Alzheimer's disease (AD). Aducanumab is a human monoclonal antibody that targets both soluble Aβ oligomers and insoluble fibrils, making it the first drug to address the underlying biology of AD. The drug's efficacy was evaluated in two identical, contemporaneous phase III trials, EMERGE and ENGAGE. In March 2019, these trials were halted based on an interim futility analysis that predicted they would miss the primary endpoint, which is the slowing of cognitive decline as measured by the Clinical Dementia Rating-Sum of Boxes (CDR-SB). The CDR-SB is a scale measurement that assesses overall cognitive ability.

In October 2019, Biogen announced that a subsequent analysis of the EMERGE trial with a larger dataset showed the trial had met its primary endpoint, leading the company to file for regulatory approval of aducanumab in the United States in 2020. During the approval process, the FDA was under the pressure from patient advocacy organizations and the agency acknowledged the importance of patients' opinions, which were overwhelmingly in favor of the drug's approval. However, the evidence supporting its efficacy was meager. While there is strong evidence that aducanumab reduces amyloid load, the correlation between plaque accumulation and cognitive decline remains uncertain. Additionally, the ENGAGE trial failed to demonstrate any benefit, resulting in

concerns about the reliability and reproducibility of the claimed efficacy of this drug. Furthermore, after 78 weeks on the highest dose, patients only showed a statistically significant, yet small, slowing of cognitive decline. The number translates into three months' worth of delay in decline over a year, and there is a lack of consensus on what constitutes clinical meaningfulness [11, 12]. Lastly, the accompanied risk of adverse events was concerning: 41.3% of patients on the highest dose developped amyloid-related imaging abnormalities (ARIA), implying vasogenic edema and intracerebral hemorrhage [13]. Accordingly, FDA required a phase IV confirmatory trial to clarify the benefits and risks associated with this drug.

On January 6, 2023, the FDA authorized the most recent treatment, lecanemab. Like aducanumab, lecanemab is a monoclonal antibody that selectively binds to large, soluble Aβ protofibrils. The phase 3 trial enrolled 1,795 symptomatic patients with early AD. After 18-month of treatment, the primary outcome measure, Clinical Dementia Rating–Sum of Boxes (a scale used to characterize cognitive and functional performance), was highly statistically positive. Key secondary outcomes, including amyloid burden on PET and several other scoring criteria for cognitive dysfunction, were all positive [14]. Lecanemab treatment may be appropriate for patients with mild AD and MCI due to AD, which is the same population enrolled in the clinical trials. However, like aducanumab, lecanemab is associated with an increased risk of ARIA. The FDA requires a series of brain MRIs during the course of treatment to monitor such side effect.

2. Risk factors for AD

The prevalence of AD increases dramatically with age. While 5.0% of people aged 65 to 74 have AD, this percentage more than doubles in the 75 to 84 age group, and doubles even further for individuals over the age of 85 [3]. Aging features a time-dependent, progressive deterioration of physiological integrity. Nine hallmarks of aging have been identified, including genomic instability, telomere attrition, epigenetic alterations, loss of proteostasis, deregulated nutrient sensing, mitochondrial dysfunction, cellular senescence, stem cell exhaustion, and altered intercellular communication [15]. Although some of these hallmarks overlap with the pathophysiological changes observed in AD, it is important to note that AD is not normal aging, and old age alone is not sufficient to cause AD. The divergence of healthy and pathological aging remains poorly characterized. Given the intertwined nature of the two processes, the advance in aging biology research continues to provide new insights and directions for AD therapeutic development.

Established genetic causes of AD include dominant mutations on genes encoding amyloid precursor protein (*APP*), presenilin 1 (*PSEN1*), and presenilin 2 (*PSEN2*). These rare mutations lead to early onset familial AD, which accounts for less than 1% of total cases. Another strong genetic risk factor for AD is the presence of *APOE* ε4 allele. *APOE* is polymorphic, and three alleles has been described: ε2, ε3 and ε4. Heterozygosity of ε3 allele increase the risk of AD by 3-fold, which homozygosity increases this risk by 12-fold [16].

Additionally, observational studies have identified a wide range of acquired, potentially modifiable risk factors of AD, including metabolic syndrome, cardiovascular

diseases, psychosocial factors, and health lifestyle choices [17, 18]. There is a strong association between AD and mid-life obesity, as well as type II diabetes, which is in line with the observation that AD brain features glucose hypometabolism and insulin resistance. Cardiovascular risk factors have also been implicated. For example, a history of stroke, which significantly associates with hypertension and heart disease, also significantly associated with the development of AD [19]. Additionally, a retrospective study has identified a declining trend of AD incidence among participants in the Framingham Heart Study. This temporal trend is in parallel with a substantial improvement in cardiovascular health [20].

Most of the risk factor for cardiovascular disease and metabolic syndrome are best managed through a general practice of healthy lifestyle, including but not limited to balanced diet, appropriate daily physical activities, sleep quality, and management of perceived stress. Therefore, focusing on a single lifestyle choice may not be sufficient. A holistic approach that promotes overall wellbeing may be more effective to make the brain resilient to cognitive decline.

The neuropathological changes in AD and related dementia are complex and multifaceted. They involve the accumulation of amyloid beta (Aβ) plaques and neurofibrillary tangles composed of tau protein. The following sections will provide a brief review of Aβ and a detailed description of tau, with a special focus on tau-implicated nuclear changes observed in AD.

3. Aβ

Aβ is a short peptide cleaved from amyloid-beta precursor protein (APP). APP is comprised of a large extracellular glycosylated N-terminus, a single transmembrane domain, and a short cytoplasmic C-terminus. Human APP can be processed in two alternative pathways: nonamyloidogenic and amyloidogenic. In the non-amyloidogenic pathway, α-secretase first cleaves the APP within the Aβ domain, separating the extracellular fragment from the membrane-tethered C terminal fragment (CTF). The CTF is then further processed by γ-secretase with the plasma membrane. On the other hand, the amyloidogenic pathway involves sequential cleavage of β-secretase and γ-secretase: the CTF generated by β-secretase can be further processed by γ-secretase at multiple sites, leading to the formation of Aβ of various lengths. The most prevalent forms of Aβ are the 40-amino-acid Aβ40 and the 42-amino-acid Aβ42.

Mutations in the human *APP* gene can cause early-onset familial AD. These mutations favor the cleavage of γ-secretase, resulting in either an increased ratio of Aβ42/Aβ40 or increased total amount of Aβ peptides. Similarly, other AD-causing mutations found on *PSEN1* and *PSEN2*, which encode protein subunits of γ-secretase, also increase the Aβ42/Aβ40 ratio. Additionally, individuals with trisomy 21 (Down's syndrome) harbor three copies of *APP* are at a substantially higher risk of AD than the general population. Rare individuals with a duplication of the *APP* locus, but not the rest of the chromosome, develop early-onset AD [21]. Contrarily, a partial trisomy that results in only two copies of *APP* lead to Down's syndrome, without AD features [22].

The aggregation of Aβ into long, unbranched fibrils is a hallmark of AD. Although earlier studies pointed to Aβ fibrils as the disease-propagating agent, more recent

investigations have suggested that soluble, oligomeric species of Aβ (AβO) inflict the most harm to neurons. AβOs have been shown as a ligand to various receptors at the plasma membrane, including but not limited to, p75 neurotrophin receptor [23], cellular prion protein [24], α subunit containing nicotinic acetylcholine receptor [25, 26], and NMDA receptor [27, 28]. These ligand-receptor interactions are proposed to transduce various neurotoxic signals into neurons, resulting in overall cellular dysfunction. Additionally, AβOs have been linked to numerous other harmful effects, including increased oxidative stress, mitochondrial dysfunction, chronic inflammation, and more.

The genetic evidence, plus demonstrated toxicity of Aβ, have culminated to the proposal of the amyloid hypothesis [29, 30]: the fundamental cause of AD is the deposition of extracellular Aβ peptides, and other neuropathology is the downstream consequence of this central event. However, the presence of senile plaque is not an exclusive feature of AD, as many individuals without notable cognitive decline possess abundant Aβ deposits in the brain. Additionally, the density of senile plaque correlates less strongly with the severity of AD, then does that of neurofibrillary tangles. It is conceivable that both Aβ-dependent and Aβ-independent mechanisms contribute AD to pathogenesis. However, the connection among Aβ, tau and other factors like ApoE remains incompletely understood.

4. Expression and structure of tau

Human tau is encoded by the microtubule-associated protein tau gene, *MAPT*, located on chromosome 17q21[31]. The primary transcript consists of 16 exons. Six isoforms of tau exist in the adult human brain, all of which results from alternative splicing of exon 2

(E2), E3 and E10 from the same transcript. E2 and E3 each encodes a 29-residue insert near the amino terminus. The isoforms containing 0,1 and 2 inserts are known as 0N, 1N and 2N tau. E10 encodes an additional microtubule binding repeat (MTBR) near the carboxyl terminus. The inclusion or exclusion of this exon differentiates between 3R and 4R tau (the second MTBR is encoded by E10).

Tau is predominantly an intracellular protein, mainly expressed in neurons in the brain and to a much less extent in oligodendrocytes[32]. Adult human neurons from periphery nervous system also express tau, but sometimes with a large additional exon (termed 4a) that doubles the size of the protein[33].

The overall amino acid composition of tau is notably hydrophilic, with 2N4R tau contains 80 serine or threonine residues, 56 negatively charged (glutamate or aspartate), 58 positively charged (lysine or arginine), and 8 aromatic (5 tyrosine and 3 phenylalanine, no tryptophane) residues. This distribution of charge is asymmetrical, with the ~120 N-terminal residues predominantly acidic (the presence of two inserts increases this feature), and the ~40 carboxy-terminal residues roughly neutral. This charge distribution plays an important role in the native structure of tau, as well as its misfolding and interactions with microtubule and other partners.

The structure of tau can be divided into several regions based on their amino acid profile and microtubule binding ability. These include the N-terminal projection domain, the C-terminal assembly domain containing the repeat domains and flanking regions, and a proline-rich region that links between the two domains.

In its monomeric form, tau is intrinsically disordered, lacking defined secondary and tertiary structures. Nuclear magnetic resonance reveals the existence of only transient α-

helix, β-strand, and polyproline II structures[34]. Small-angle X-ray scattering also shows that tau possesses features similar to random coils[35]. However, the absence of stable local structures does not preclude the possibility of global, long-range interactions. When unbound to microtubules, tau assumes a paperclip-like conformation in which the N-terminal and C-terminal regions fold back and stay in close proximity to each other[36]. It's worth noting that this interaction is fluctuating and lacks the character of a firm docking of two binding sites that results in substantial immobilization.

5. Tau aggregation and toxicity

The core of the PHFs associated with tauopathies consists of β-sheets that coincide with repeat domains of tau, which are surrounded by a fuzzy coat made up of unstructured C-terminal and N-terminal domains [37]. The structure of the fuzzy coat resembles a two-layered, anionic polyelectrolyte brush. The mechanical and adhesive properties of the fuzzy coat are influenced by post-translational modifications, local pH and electrocyte concentrations, which affect the aggregation propensity of tau [38]. Two hexapeptide sequences, ^{275}VQIINK^{280} and ^{306}VQIVYK^{311}, at the beginning of repeat domains 2 and 3, respectively, are required for the self-aggregation of tau protein [39]. The local clustering of V, I, Y, and Q supports hydrophobic interactions that stabilize β-sheet formation. Indeed, ^{306}VQIVYK^{311} itself is sufficient to form fibrils, whose fundamental unit is a steric zipper formed by two tightly interdigitated β-sheets [40]. Mutations related to FTD, such as ΔK280 and P301L, which promote β-sheets formation even further, have been observed to accelerate tau aggregation both *in vitro* and *in vivo.*

Conversely, proline mutations in the hexapeptide motifs, which are considered as β-sheets breaker, inhibit tau aggregation *in vitro* [41].

Tau aggregation can be accelerated by various cofactors, including polyanions and anionic micelles. Heparin [42], RNA [43], and arachidonic acid micelles [44] have been shown to induce aggregation of recombinant tau *in vitro*. These negatively charged cofactors reduce the repulsion between the cationic residues on tau molecules, enhancing the local concentration of the protein and promote its aggregation. While co-factor-induced tau fibrillization has been a useful model for characterizing the biochemical processes and structure of tau aggregation, the bio-relevance of such tau aggregates has been questioned. Cryo-electron microscopy study has revealed that the structure of heparin-induced fibrils from full length tau differs from that of filaments extracted from human brains[45]. A recently published protocol has demonstrated that tau can be efficiently aggregated into seeding-competent fibrils in the absence of co-factor [46]. This is a valuable methodology to model tau aggregation *in vitro*, without potential artifacts from the involvement of cofactors.

Tau aggregation is a complicated process influenced by a multitude of factors *in vivo*. For example, post-translational modifications (PTMs), such as acetylation, methylation, and glycosylation, have been found on tau and their effects on tau aggregation are still being investigated. Hyperphosphorylation is a characteristic of aggregated tau species extracted from transgenic mice, human brains affected by AD and other tauopathies. However, the impact of phosphorylation on pathological tau aggregation is still a matter of debate, partly due to heterogeneous phosphorylation patterns on tau. For example, combined phosphorylation at the Ser202/Thr205/Ser208 is sufficient to induce tau

aggregation and the fibers are detectable by thioflavin fluorescence or electron microscopy *in vitro*. But phosphorylation at Ser262 can interfere with this combinatory effect[47, 48]. Furthermore, PHF-like phosphorylation of tau was detected in hibernating animals, without any evidence of neurofibrillary aggregations [49], indicating that phosphorylation alone is not sufficient to initiate aggregation. It is possible that tau aggregation is triggered by unknown factors *in vivo* and the rate is indirectly modulated by different phosphorylation patterns. In fact, mass spectrometry analysis of PHFs extracted from AD brains revealed that phosphorylation occurred largely in the fuzzy coat, while the structural core components of the PHF were mostly acetylated or ubiquitinated [50].

Truncated fragments of tau protein that contain the MTBR region have a high tendency to aggregate, probably due to the disruption of the paperclip conformation, in which the repeated domains are shield by the N- and C-terminal tails. Since first reported in 1993, over 50 abnormally cleaved tau fragments have been identified in the brains of individuals with AD , although many of these fragments are not yet well characterized [51]. One such fragment, $Tau_{151–391,}$ which was identified as the core of PHF by pronase digestion (degrades the fuzzy coat) [37], has been found to be prone to aggregation *in vitro* [52, 53]. In AD human brain and P301S transgenic mice, asparagine endopeptidase was hyperactivated, leading to the cleavage of tau at both N255 and N368 residues. Thioflavin assays have shown that $tau_{256–368}$ displays higher propensity for aggregation in the presence of heparin *in vitro*, compared to full-length tau [54].

Tau aggregation is the hallmark of several neurodegenerative disease collectively known as tauopathies, with AD being the most common form. While tau plays an important role in the pathogenesis, it has become evident that the presence of neurofibrillary tau tangles, which are bundles of PHFs, is not sufficient to cause neuronal dysfunction. For example, *in vivo* two-photon calcium imaging has demonstrated that neurons in the visual cortex from rTg4510 mice, which bear NFTs, function normally. They were found to maintain a normal baseline calcium level and were able to integrate dendritic inputs and respond to visual stimuli [55]. Additionally, suppressing the tau transgene in this mouse strain has been shown to improve cognitive function, even when NFTs were already prevalent [56]. Meanwhile, research started to investigate the neurotoxicity of soluble, oligomeric tau species. Oligomeric tau has many damaging effects, such as disturbing energy production and mitochondrial function, destabilizing microtubules, altering neuronal cytoskeletons and axonal transport [57]. Therefore, the formation of NFTs and PHFs might be a protective response: they scavenge and sequester more toxic oligomeric tau species, which have broad deleterious impacts on various cellular processes.

The relationship between amyloid, tau, cognitive functions, and AD is complex and multifaceted. A growing body of evidence suggests that amyloid provokes or facilitates the development of tau pathology, which ultimately leads to cognitive impairments. Indeed, tau burden correlates better with cognitive deficit than does amyloid [58, 59]. However, in pure tauopathies, pathological tau spread through the brain in the absence of amyloid. Moreover, a recent study has identified four distinct trajectories of tau deposition in AD, each with different cognitive profiles and longitudinal outcomes [60].

Therefore, the trigger of tau pathology remains unclear, and the way it spreads can vary significantly between individuals. The recently developed spatial transcriptomic analysis has the potential to provide valuable insights into how amyloid and tau interact and interfere with normal physiology at the single cell level, as well as identify whether there is a differential pattern based on the spatial distribution of tau pathology.

The upcoming sections will discuss some key functions of tau in the neuronal nucleus and perinuclear region, in both physiological and pathological contexts.

6. Tau in the nucleus

In healthy neurons, tau primarily associates with microtubules, thereby regulating microtubule dynamics and axonal transport. Tau exhibits a polarized distribution in neurons and the retrograde diffusion barrier coincides with the axon initial segments (AIS) [61]. Interestingly, the sorting of tau appears to be isoform-dependent, with 1N isoforms being strongly localized to the neuronal nucleus, while 0N isoforms are predominantly axonal [62]. Notably, tau lacks any nuclear localization signals, which would allow for translocation from cytoplasm to the nucleus. However, a recent paper reported the existence of a putative NLS sequence between amino acids 141 and 178 of tau. including an importin-α binding site. The translocation seems to require tau phosphorylation as well. Wild type tau transfected into HEK cells almost entirely localizes to the cytoplasm, whereas tau harboring pseudo-phosphorylation sites (S199E, T212E, T231E, and S262E) was able to enter the nucleus [63].

Inside the nucleus, tau has been reported to interact with DNA, protein components associated with chromatin, and RNA, both in normal physiology and pathology. *In vitro*

binding analysis demonstrated tau's ability to interact with DNA and chromatin [64]. Recent *in vivo* analysis has shown that neuronal nuclear tau interacts with pericentromeric heterochromatin (PCH). The clustered distribution of PCH is disrupted in neurons derived from tau knock-out mice, accompanied by an abnormal accumulation of stress-induced PCH DNA breaks [65]. Moreover, tau plays a crucial role in preserving DNA and RNA integrity under hyperthermia conditions that induce ROS-related stresses [66].

On the other hand, an early work from the Binder group indicates the existence of tau in the nucleolus of the human neuroblastoma cells, as revealed through Tau-1 immunofluorescence [67]. Given that nucleolus is crucial in regulating rRNA gene metabolism, later studies further investigated the potential involvement of tau in ribosomal RNA transcription and ribonucleoprotein complex formation. Chromatin immunoprecipitation (ChIP)-qPCR revealed that tau specifically interacts with ribosomal DNA that encodes 45S pre-rRNA. To confirm that tau presence regulates rRNA synthesis, the authors also showed that stable or transient tau-depletion significantly decreased rDNA transcription level in human embryonic kidney HEK293T cells [68]. Furthermore, the human tau interactome analysis has revealed a robust association of the tau protein with the ribonucleoproteome [69]. More specifically, RNA-binding proteins Musashi has been reported to mislocalize and associate with oligomeric tau species in AD and FTD [70].

Lastly, pathological tau also interacts with various components on the nuclear membrane, which we will review in detail in the following sections.

7. Nuclear lamina deformation in AD and related tauopathies

Nuclear envelope (NE) serves as the boundary of the cell nucleus. Comprised of two membranes – the outer and inner nuclear membranes (ONM and INM) – the NE is perforated with nuclear pore complexes (NPCs) that allow for the selective transport of macromolecules between the nucleus and cytoplasm.

The ONM, which faces the cytoplasm, is continuous with the rough endoplasmic reticulum (ER). Meanwhile, the INM faces the nucleoplasm, which is associated with an underlying meshwork of protein, termed nuclear lamina. Nuclear lamina plays crucial roles in supporting nuclear structure and its mechanics, as well as chromatin organization and gene expression.

The major component of the lamina is lamin, a type V intermediate filament protein that contains a central α-helical coiled coil domain [71]. The assembly of the lamina begins with the dimerization of the coiled-coil domains. These dimers polymerize head-to-tail to form long threads that eventually associate into fibers, which then form higher-order lattices.

In humans, there are three genes encoding lamin protein: *LMNA* (coding for lamin A and lamin C proteins), *LMNB1* (lamin B1), and *LMNB2* (lamin B2). B-type lamins are constitutively expressed in most cell types, whereas A-type lamins are developmentally regulated.

B-type lamins are indispensable for brain development and postnatal neuron survival. Lamin B2-deficient mice die at birth. Histopathological analysis did not uncover any other organ abnormalities, except for the brain, where a dramatic layering defect was found in the forebrain [72]. Lamin B1-deficiency is also perinatal lethal in mice, with

defects in bones, lungs, and brain cortical layering organization [73, 74]. In most periphery tissues, the levels of lamin A and C are similar. However, the expression of lamin A is much lower in the mouse central nervous system, because the prelamin A transcript is eliminated by miR-9 microRNA [75, 76]. This expression pattern is consistent with the fact that patients of *LMNA*-linked progeria disorders do not suffer from dementia, even though these syndromes mimic physiological aging at an early age.

The relationship between nuclear lamina and neurodegeneration was first described by Frost et al., in a transgenic human tau *Drosophila* model. They found that pathological tau induced overstabilization of F-actin disrupts LINC complex organization and lamina deformation, which promotes heterochromatin relaxation and DNA damage accumulation [1]. Lamin pathology is conserved in post-mortem human Alzheimer's disease brains. Immunohistological analysis showed a significant number of neurons in AD brains harbored lamina invagination, as well as a reduction of lamin B1 protein level, as measured by fluorescence intensity of the staining [1]. However, a later study showed that in late-stages of AD, *LMNA* mRNA level was up-regulated in the hippocampal tissue, while the level of *LMNB* mRNA was comparable to that of the controls [77]. A recent study proposed the idea that the disruption of nuclear envelope integrity is a possible initiating event in tauopathies [78]. The genetic screen was done for identifying mutations that promote or inhibit tau aggregation in HEK293T biosensor cell line, which has been engineered to report tau seeding activity. The initial screen yielded three genes, *BANF1*, *ANKLE2*, and *PPP2CA*, whose inactivation promotes tau accumulation. The protein-protein association network analysis showed the proteins encoded by these genes are functionally involved in the maintenance of the nuclear envelope [78]. Knock-down

of *BANF1*, *ANKLE2*, and *PPP2CA* in primary mouse neuron cultures caused a significant increase in tau phosphorylation at serine 356 and impair nuclear envelope integrity, as shown by apparent leakage of nuclear localized fluorescent protein (NLS:mCherry) into the perinuclear region [78]. Overall, these findings suggest that nuclear envelope dysfunction and laminopathy may play a critical role in the pathogenesis of neurodegenerative diseases.

8. Nuclear pore complex defects in AD and related tauopathies

NPCs are the only channels that allow regulated traffic of molecules between the nucleus and the cytoplasm. These giant macromolecular assemblies have an outer diameter of ~120-130 nm and a height of 50-80 nm. The core of the NPC consists of eight spokes arranged in rotational symmetry around a central channel. The spokes are connected to three rings: an inner ring in the plane of the nuclear envelope, sandwiched by two outer rings at the cytoplasmic and nucleoplasmic surfaces. Protein filaments extend from the outer rings, form cytoplasmic-facing mRNA export platform and nucleoplasmic-facing nuclear basket. Each ring is composed of multiple copies of different nucleoporins (Nups).

Nups are the basic building blocks of NPC, which can be classified into three categories: transmembrane Nups that anchor the NPC to the nuclear membrane, scaffold Nups that form layered ring structures, and channel Nups that line the central pore. Channel Nups project intrinsically disordered, phenylalanine-glycine (FG) rich protein segments into the channel pore, creating an entropic barrier that helps with selective transport of molecules through the NPC.

The practical permeability limits of NPC have been defined by diffusion assays: fluorescently labeled dextrans or gold particles, microinjected into cells, have shown that macromolecules greater than 40 kDa do not show any measurable redistribution between the nucleus and cytoplasm within physiological time scales, [79, 80]. In fact, larger cargoes require regulated active transport through NPC, relying on nuclear transport receptor and Ran gradient. This type of translocation requires, at minimal, a shuttling receptor and transport signals on the cargo protein, including nuclear localization sequences (NLSs) and nuclear export sequences (NESs). Most shuttling receptors belong to protein family called karyopherins, which are also known as importins, exportins, or transportins. Karyopherins not only binds to cargo directly (though sometimes requires an adaptor), but also to the NPC and small Ras-like GTPase Ran.

The directionality of karyopherin-facilitated transport is defined by the gradient of Ran protein, a small GTPase from the Ras superfamily. This gradient is generated by the asymmetric cellular distribution of regulators of the RanGTPase: Ran GTPase activating protein (RanGAP) concentrates in the cytoplasm and the Ran guanine nucleotide exchange factor (RanGEF) in the nucleoplasm. Therefore, RanGTP concentration is higher in the nucleus and lower in the cytoplasm, providing the energy for nuclear transport via hydrolysis of RanGTP. The import process can be divided into three steps: (1) recognition of the cargo by RanGDP-bound importin via its NLS sequence, forming an importin-cargo complex; (2) docking of the complex to the NPC by binding to FG-Nups, followed by translocation to the nucleus; and (3) dissociation of the complex, triggered by RanGTP interaction with the importin. RanGTP-bound importin is then shuttled outside to the cytoplasm, where GTP hydrolysis, stimulated by RanGAP, frees

the importin from RanGDP. In the case of export complexes, an analogous process occurs, but RanGTP binding on the nucleoplasmic side enhances the affinity of the exportin to the cargo. Cells control the export of RNA from the nucleus in a similar fashion. As transcription and splicing proceed, nascent RNA transcripts associate with various protein containing NES that are recognized by exportins, leading to the transport of mRNA- protein complex. Upon entering the cytoplasm, GTP hydrolysis triggers to the dissociation of protein-coating and mRNA.

Alterations in nucleocytoplasmic transport has been associated to AD and tau mediated FTD. Electron microscopic studies of AD post-mortem hippocampal tissues have revealed that tangle-bearing neurons frequently exhibited irregular nuclei and prominent clusters of nuclear pores [81]. Importin α, an essential component of cytoplasmic-nuclear transport, has been found to accumulate in hippocampal CA1 neurons of individuals with AD [82]. Moreover, defects in nuclear pore morphology and function have been observed with AD. Immunohistochemical analysis has shown that Nup98, an FG-rich nucleoporin, mislocalizes to the cytosol and closely associates with hyperphosphorylated tau in AD brain tissue, leading to nuclear leakiness and import/export defects. Dextran permeability assays have demonstrated impaired nuclear transport in AD brain tissue, as isolated nuclei from cortices exhibited influx of 70-kDa dextran and partially of 500-kDa dextran, whereas nuclei from AD cerebellum tissue (devoid of tau pathology) excluded both dextran dyes. In primary mouse neurons, exposure to high molecular weight tau derived from AD human brain tissue leads to mislocalization of fluorescent proteins fused to nuclear import or export signals, indicating impaired active nuclear transport. [83].

Similarly, in cortical neurons differentiated from induced pluripotent stem cells (iPSCs) of individuals harboring FTD-causing tau mutations, there is a higher incidence of lamina invaginations. Deformation of the nuclear membrane is actively mediated by microtubules, as live imaging has revealed that microtubules abnormally project into the nuclei of these neurons, Treatment of nocodazole, a microtubule depolymerization agent, restores the round nuclear morphology [84]. The authors also demonstrated that nucleocytoplasmic transport is defective in these neurons, by ectopically expressing the NES:GFP and NLS:RFP from a single construct in iPSC-derived neurons.

9. Histone modifications and transcriptional alterations in AD

To fit into the confined space of the nucleus, genomic DNA is highly packed with the aid of proteins to form chromatin. The basic repeating subunit of chromatin if the nucleosome, whose core is an octamer containing two copies of histones H2A, H2B, H3, and H4. About 146 base pair of DNA wraps around this protein core and linker histone H1 stabilizes the structure at the entry and exit sites of DNA. The N-terminal tails of core histones extend from their globular domains and undergo post-translation modifications, including acetylation, methylation, phosphorylation, and sumoylation. PTMs contributes significantly to epigenetic regulation of gene expression.

A growing body of evidence suggests that epigenetic alteration, such as histone modifications, plays a major role in AD pathogenesis. In post-mortem AD brains, Enzymes responsible for the removal or addition of specific histone modifications exhibit varying levels of expression. Moreover, heterochromatin directly interacts with nuclear lamina with its lamina-associated chromatin domains (LADs). Deformation of the

nuclear lamina may therefore disrupt chromatin organization, ultimately impacting transcription profiles. Here we focus on histone acetylation and methylation, the two most well-studied forms of histone modification in neurodegenerative diseases.

Histone acetylation is carried out by histone acetylases (HATs) and reversed by histone deacetylases (HDACs). Acetylation of lysine residues neutralizes their positive charge and eliminates its interaction with negatively charged phosphate group on the DNA. This results in a less compact chromatin structure, which is more accessible to transcriptional machinery, and leads to gene activation. Histone acetylation is thus closely associated with gene transcriptional activation.

Histone acetylation changes have been implicated in AD pathogenesis. Early studies have reported elevated expressions of HDAC6 and HDAC2 in the brains of individuals with AD [85, 86] and a more recent study found higher levels of histone 3 lysine 14 acetylation (H3K14ac) in post-mortem brains from end-stage AD patients [87]. With the development of ChIP-seq, it has become possible to evaluate genome-wide acetylation patterns in post-mortem AD brain tissue. A recent study investigated genome-wide H3K9ac pattern, a histone mark for open chromatins that are transcriptionally active, in 669 aged human prefrontal cortices. They found that H3K9ac remodeling aggregates into large segments that associates with nuclear lamina. Computational modeling showed that differential peaks of H3K9ac strongly associate with tau pathology, which was validated by *in vitro* experiments. Over expression of tau in human neurons derived from induced pluripotent stem cells recapitulated such identified changes [88]. Not all epigenetic changes translate to transcriptional alterations. A recent integrated multi-omics approach, combining transcriptomic, proteomic and epigenomic analyses, has revealed an

upregulation of transcription- and chromatin-related genes, including the histone acetyltransferases for H3K27ac and H3K9ac. By analyzing post-mortem human AD brains, this study also confirmed the disease-specific enrichment of H3K27ac and H3K9ac, identifying them as potential epigenetic drivers of AD [89].

Histone methylation is achieved by histone methyltransferases (HMT) and is reversed by histone demethylase. Methylation can occur on all basic residues: lysine can be mono-, di-, or tri- methylated; arginine can be monomethylated, symmetrically dimethylated, or asymmetrically dimethylated; histidine can be monomethylated. The effect of methylation is context dependent. For example, H3K9me2/3 and H3K27me3 are markers for heterochromatin, whereas H3K4me3 is generally associated with active transcription.

The role of histone methylation changes in AD is not yet fully understood. Frost et al. reported a widespread loss of H3K9me2 and HP1α, markers for heterochromatin, in the brains of tau transgenic *Drosophila*, tau transgenic mice and human AD hippocampus [90]. Follow-up study revealed that relaxation of constitutive heterochromatin leads to dysregulated activation of transposable elements in AD and associated tauopathies [91]. In contrast, Zheng et al. identified significant decrease of H3K9me2 in post-mortem human AD prefrontal cortices and in 5XFAD mouse model. H3K9me2 ChIP assay showed genome-wide increase of histone methylation in 5XFAD mice compared to WT controls [92]. Additionally, Lee et al. reported that H3K9me3-dependent heterochromatin condensation is robustly elevated in the end-stage sporadic AD post-mortem temporal cortices. Subsequent H3K9Me3 ChIP-seq and mRNA-seq identified that the differential H3K9Me3 enrichment patterns inversely correlate with mRNA expression levels in AD

and downregulated genes mainly involved in synaptic transmission [93]. Another ChIP-seq study was conducted on H3k4me3 and H3k27me3 in post-mortem entorhinal cortex tissues from 15 elderly individuals, including 6 AD cases and 9 age-matched control. The results showed a decrease in overall H3k4me3 signal in AD cases and a concomitant increase of H3k27me3 signal, especially in males [94].

It's important to recognize that AD is marked by the selectively vulnerability of certain groups of cells. Therefore, conducting a bulk-tissue analysis may mask the intricacy of changes that occur among various cell subpopulations, especially less abundant cell types. To overcome this limitation, single-cell RNA sequencing (scRNA-seq) offers an alternative approach for investigating the diverse cellular response to pathological changes. Recent studies have combined snRNA-seq with single nucleus assay for transposase-accessible chromatin with sequencing (snATAC-seq). By correlating chromatin accessibility with nearby gene expression, researchers can identify cell-type specific *cis*-regulatory elements and associated transcription factor unique to AD human brain [95, 96]. Multi-omics approach is powerful to identify previously unidentified targets in AD. For example, ZEB1, a transcription factor important for epithelial-mesenchymal transition in cancer, has been found to be enriched in both AD-specific neuronal and glial populations [96]. Further research is needed to unravel its role in neurodegeneration.

Chapter 2

Structural and functional damage to neuronal nuclei caused by extracellular tau oligomers

The following chapter has been adapted and expanded from a publication by Sun, et. al.

Introduction

Oligomeric and filamentous tau are key pathogenic factors in tauopathies, such as Alzheimer's Disease (AD), frontotemporal dementia (FTD), and progressive supranuclear palsy (PSP). Tauopathy spreads from neuron to neuron by cycles of tau aggregate release into the extracellular space and subsequent neuronal uptake [97-102]. While the mechanisms of this prion-like spread of pathogenic tau have been extensively studied, the cell biological responses of neurons to aggregated tau uptake have attracted much less attention.

The nuclear lamina, a meshwork of intermediate filaments underlying the inner nuclear membrane, plays critical roles in the maintenance of normal nuclear structure and function. Deformation of the nuclear membrane, including nuclear lamina invagination, has been implicated in multiple neurodegenerative diseases, including AD, FTD, and Parkinson's disease, and can be provoked by dysfunctional tau [1, 84, 103]. For example, expression of pathogenically mutated human tau in *Drosophila* neurons caused nuclear lamina invagination [1], and intracellular tau oligomerization led to the disassembly of lamin B2, one of the major components of nuclear lamina [104].

With this background in mind, we investigated whether extracellular tau oligomers (xcTauOs) affect neuronal nuclei. We provide evidence that xcTauOs rapidly cause striking nuclear invagination by a mechanism that depends on intracellular tau, and is associated with disrupted nucleocytoplasmic transport, and altered chromatin structure

and gene transcription. Altogether, our results implicate xcTauOs as seminal factors in the conversion of healthy neurons into diseased neurons in AD and other tauopathies.

Materials and Method

1. Human brain tissue

Paraffin-embedded, 5-6 μm thick human cortical brain autopsy sections were obtained from the archives of the University of Virginia Department of Pathology. Frozen human cortical brain autopsy samples were provided by Dr. Heather A. Ferris of the University of Virginia School of Medicine. Pertinent information about each donor is shown in Supplementary Table 1. Institutional approval for use of archival autopsy tissue was obtained from the University of Virginia Biorepository and Tissue Research Facility.

2. Mouse brain tissue

CVN mice were originally obtained from Drs. Michael Vitek and Carol Colton of Duke University and were maintained as a breeding colony. PS19 mouse brain sections were provided by Dr. John Lukens of the University of Virginia Department of Neuroscience. Animals were maintained, bred, and euthanized in compliance with all policies of the Animal Care and Use Committee of the University of Virginia. 50 μm floating sections of brain tissue were cut following trans-cardiac perfusion of 4% paraformaldehyde in PBS of mice that had been deeply anesthetized intraperitoneally with ketamine/xylazine (280/80 mg/kg).

hTau mice were originally obtained from the Jackson Laboratory and maintained as a breeding colony. Mice were euthanized by carbon dioxide inhalation. The brains were then harvested and saved at -80°C for future use. For all experiments, only male mice were used.

3. Cultured mouse neurons

Brain cortices were collected from E17/18 wild type (WT) C57/Bl6 or tau knockout mice [105] and processed as described earlier [106]. Briefly, brain tissue was cut into small pieces in ice-cold Hank's balanced salt solution, and then was digested at 37°C with 0.25% trypsin (Gibco, 15090-046) and 500 units DNase (Worthington, LK003170) for 20 minutes. Digestion was stopped by adding equal volume of fetal bovine serum. The resulting single cell suspension was washed three time with 5 ml of warm Neurobasal Plus medium (Gibco, A3582901) containing B27 Plus supplement (Gibco, A3582801), 2mM GlutaMAX (Gibco, 35050061), 6mg/ml glucose (Sigma-Aldrich, 16301) and 10 µg/ml gentamicin (Gibco, 15750078), mechanically dissociated with a fire polished Pasteur pipet and diluted into supplemented Neurobasal Plus medium. 65000 cells/cm^2 were plated on 50 µg/ml poly-D-Lysine (Sigma-Aldrich, P0899) coated plates. Neurons were maintained in a tri-gas incubator in an atmosphere of 5% each of O_2 and CO_2. 50% media changes were done every 3-4 days until day 12 or 13 when experimental treatments began.

4. Recombinant tau

All 6 human tau isoforms with a C-terminal his-tag were produced by expression in BL21(DE3) *E. coli* cells. Protein expression was induced with 0.5 mM Isopropyl β-D-1-thiogalactopyranoside (Sigma-Aldrich, I6758) for 2 hours at 37°C. Cells were pelleted by centrifugation, resuspended and sonicated with Misonix Sonicator 3000 20 times for 30 seconds each at 60% power. Next, the *E. coli* lysate was centrifuged in a Sorvall RC6 Plus 6 centrifuge at 10,900 rpm for 25min with an SLA 1500 rotor. Tau was then purified

batchwise from the supernatant using TALON Metal Affinity Resin (TaKaRa, 635502) according to the vendor's instructions. Finally, each purified tau isoform was concentrated, and buffer exchanged into 10mM HEPES, pH 7.6, using Amicon Ultra-4 Centrifugal Filters (Millipore, UFC801024).

5. Tau oligomers

Oligomeric tau was prepared as described earlier [107]. Each purified tau isoform was adjusted to 8 μM in the oligomerization buffer: 10 mM HEPES (pH 7.6), 100mM NaCl, 0.1 mM EDTA and 5mM DTT. The protein was then allowed to oligomerize in the presence of 300μM Arachidonic acid (Cayman Chemicals, 90010) for 18 hours at room temperature in the dark. Oligomerization was verified on western blots. Primary mouse neurons at 12-13 days *in vitro* were exposed to oligomeric or monomeric tau at 30-500 nM total tau, or with vehicle for the indicated time periods.

6. Lentivirus production and transduction

Human 2N4R tau cDNA was amplified by PCR and transferred to the FSW lentiviral vector between the BamHI and HpaI sites. Primers was described earlier [108]. The expression plasmids encoding tau, and the packaging vectors, (pSPAX2 and pMD2.G; (Addgene plasmids 12260 and 12259, respectively) were transfected using Lipofectamine 3000 (ThermoFisher, L3000001) into HEK293T cells grown in 15 cm Petri dishes to ~80% confluence in Dulbecco's Modified Eagle's medium (Gibco 11965-092) supplemented with 10% fetal bovine serum (VWR, 89510-186). Each transfection employed 15 μg total DNA at a 50%/37.5%/12.5% ratio of expression

vector/pSPAX2/pMD2.G. Lentivirus-conditioned medium was collected 24 and 48 hours after the start of transfection. Lentiviral particles were concentrated in a Beckman Coulter Optima LE-80K ultracentrifuge for 2 hours at 23,000 rpm at 4°C in an SW28 rotor, resuspended in 400 µl Neurobasal medium and stored at −80°C in small aliquots. Cultured neurons were transduced in Neurobasal/B27 medium and incubated for 48-72 hours before assays were performed.

7. Brain homogenate preparation

Cerebral hemispheres were dissected from freshly euthanized mice, suspended in 3 volumes of PBS at 4º C, and homogenized on ice using 25 pulses of 30 seconds each of a probe sonicator (Misonix Sonicator 3000) at 30% power. Lysates were centrifuged at 21,000 g for 15min with a TLA 120.2 rotor (Beckman Optima TLX Ultracentrifuge) to remove cellular debris and large, insoluble material. Supernatants were then passed through a 0.22 um filter, aliquoted and stored at −80 °C until further use. Total protein concentration was determined by Pierce BCA Protein Assay Kit (Thermo Scientific, 23225).

8. Quantitative immunofluorescence

All micrographs were acquired using an inverted Nikon Eclipse Ti microscope equipped with a Yokogawa CSU-X1 spinning disk confocal head with 405 nm, 488 nm, 561 nm and 640 nm lasers, and 10X and 20X dry, and 40X and 60X oil immersion Nikon Plan Apo objectives. All brain and cultured neuron immunofluorescence micrographs are

shown as maximum projections of Z-stacks produced using the Fiji derivative of ImageJ. Primary and secondary antibodies are listed in Supplementary Table 2.

Primary mouse neurons growing on coverslips were rinsed once with PBS, and with one exception, were fixed and permeabilized in methanol for 5 minutes at -20° C. The exception was that cells stained with anti-Ran were fixed with 2% paraformaldehyde for 10 minutes at room temperature and permeabilized with 0.2% Triton X-100 for 10 minutes. After washing three times with PBS, cultured neurons were blocked in Intercept (PBS) Blocking Buffer (LI-COR, 927-70001) /0.1% Tween 20 for 1 hour and incubated with the indicated primary antibodies for 30 minutes, followed by the indicated secondary antibodies for 30 minutes. All antibodies were diluted in Intercept (PBS) Blocking Buffer/0.1% Tween20. After each antibody incubation step, the cells were rinsed 3 times for 5 minutes each with PBS. In the last wash, the coverslips were incubated with 5ug/ml DAPI (Sigma-Aldrich, D9542). The coverslips were then mounted onto slides using Fluoromount-G (Southern Biotech, 0100-01). To quantify nuclear invagination in primary neurons, lamin B1-positive pixels were assigned as either nuclear boundary or invaginated using a Fiji thresholding algorithm, and nuclei were classified as invaginated if ≥ 10% of the lamin B1-positive pixels were invaginated (Figure 1A). At least 100 neurons per condition were evaluated fort each experiment.

Human paraffin embedded brain sections were first deparaffinized and rehydrated by sequential incubation in Xylenes (2 x 5 minutes), 1:1 xylenes:100% ethanol (3 minutes), 100% ethanol (3 minutes), 95% ethanol (3 minutes), 70% ethanol (3 minutes), 50% ethanol (3 minutes), and distilled water (3 minutes). Antigen retrieval was achieved by microwaving the sections in citrate buffer pH 6.0 (Vector Laboratories, H-3300) for 15

minutes. After cooling to room temperature, sections were rinsed in PBS and blocked in PBS/5% BSA/0.1% Triton X-100 for 1 hour at room temperature and incubated with the indicated primary antibodies diluted in PBS/5% BSA overnight at 4° C. Sections were then washed 4 times for 5 minutes each in PBS and incubated with the indicated secondary antibodies for 2 hours at room temperature. After washing 4 times for 5 minutes each in PBS, sections were incubated with DAPI for 10 minutes and then with autofluorescence eliminator (Millipore, 2160) for 5 minutes, followed by 3 washes with ethanol. Finally, the tissue sections were mounted under #1 thickness coverslips using Fluoromount-G. Approximately 50 MAP2-positive nuclei were evaluated in each case. A nucleus was considered invaginated if the total length of its invaginations was at least 10% of the longest axis of the nucleus.

Free floating, 50 μm mouse brain sections were rinsed in PBS for 5 minutes and blocked with PBS/5% normal goat serum (Southern Biotech, 0060-01) for 2 hours at room temperature. Sections were then incubated with the indicated primary antibodies diluted into PBS/2% normal goat serum/0.05% Tween 20 overnight at 4° C. Sections were then washed with PBS/0.05% Tween 20 3 times for 10 minutes each and incubated with the indicated secondary antibodies for 2 hours at room temperature. After three washes with PBS, the sections were incubated with DAPI for 10 minutes and autofluorescence eliminator for 5 minutes, followed with 3 washes with ethanol. After the final wash, the sections were rinsed with PBS and mounted between #1 thickness coverslips and glass slides using Fluoromount-G. To ensure thorough neuroanatomical coverage, cortical sections from anterior, middle and posterior regions were imaged and about 300 neurons from each section were evaluated. A nucleus was considered

invaginated if the total length of its invaginations were at least 10% of the longest axis of the nucleus.

9. Protein electrophoresis and western blots

For cultured neurons, total protein was extracted using RIPA buffer (Thermo Scientific, 89900) supplemented with protease inhibitors (Thermo Scientific, 78430) and phosphatase inhibitors (Thermo Scientific, 78420). Protein samples were mixed with 1X NuPage LDS Sample Buffer (Invitrogen, NP0007) and 1x sample reducing agent (Invitrogen, NP0004). Samples were heated at 70°C for 10 minutes and separated on 4-12% gradient Bis-Tris SDSPAGE gels (Invitrogen, NP0323) and transferred to 0.2µm nitrocellulose membrane (Bio-Rad Laboratories, 1620112) for 1 hour at 100V.

For human brain tissue, 50-100 mg of tissue was blended with one scoop of zirconium oxide beads (Next Advance, ZOB05) in 300ul buffer containing 65mM Tris-HCl, pH 6.8, 2.1% SDS, 5% β-mercaptoethanol and 0.1% Triton X-100 for 10 minutes. The lysate was then sonicated for 5 minutes and centrifuged at 14,000 g for 15 minutes with a accuSpin Micro 17R Centrifuge (Fisher Scientific) at 4°C. Samples were diluted 5-fold into 1x Laemmli sample buffer (Bio-Rad Laboratories, 1610747) with 5% β-mercaptoethanol. The samples were then heated at 95°C for 10 minutes, separated on 4-12% gradient Bis-Tris SDSPAGE gels (Invitrogen, NP0323), and transferred to 0.2µm nitrocellulose membrane (Bio-Rad Laboratories, 1620112) for 8 hours at 25V.

Primary and secondary antibodies for western blotting are listed in Supplementary Table 2. All antibodies were diluted in Intercept (TBS) Blocking Buffer/0.1% Tween-20. Following protein transfer, nitrocellulose membranes were blocked with Intercept (TBS)

Blocking Buffer (LI-COR, 927-60001) for 1 hour at room temperature and incubated with the indicated primary antibodies overnight at 4° C. Membranes were then washed 3 times for 5 minutes each in TBST (TBS/0.1% Tween 20) before being incubated with the indicated secondary antibodies at room temperature for 1 hour. Finally, the membranes were washed 3 times in TBST, and were imaged using a ChemiDoc MP imager and analyzed using Image Lab software (Bio-Rad).

10. Dextran Exclusion Assay

A previously described protocol [109] was adapted to primary WT mouse neurons that grew on glass coverslips and were exposed to xcTauOs (250nM total tau) or vehicle for 24 hours, and then washed once with prewarmed PBS and ice-cold PBS, respectively. Next, neurons were incubated in permeabilization buffer (20 mM HEPES pH 7.5, 110mM KOAc, 5 mM $MgCl_2$, and 0.25 M sucrose) for 5 minutes on ice, followed by a 7-minute incubation with permeabilization buffer containing 20 µg/mL of digitonin (Sigma-Aldrich, CHR103). Neurons were then washed 4 times with diffusion assay solution (20 mM HEPES pH 7.5, 110 mM KOAc, 5 mM NaCl, 2 mM $MgCl_2$, 0.25 M sucrose) on ice and incubated with 1 mg/ml of fluorescein-dextran (Invitrogen, D1823) for 10 minutes at room temperature. Hoechst 33342 was used as the nuclear counterstain (NucBlue Live ReadyProbe Reagent, Invitrogen, R37605). The glass coverslips were sealed onto slides with clear nail polish and imaged using a 20X 0.4 NA Plan Fluorite objective on an EVOS M5000 cell imaging system (ThermoFisher Scientific). Images were quantitatively analyzed using Fiji software: regions of interest (ROIs) defining nuclei region were hand drawn based on Hoechst staining, and the mean pixel intensity of

nucleus-associated fluorescein-dextran was standardized against the mean pixel intensity of the background.

11. H3K9Me3 antibody validation

Specificity of the antibody to histone H3 tri-methylated at lysine 9 was tested against two types of substrates: recombinant histone 3 (New England BioLabs, M2507S), which lacked methylation, and native histones that contain the modification and were extracted from HEK293T cells using a Histone Extraction Kit (Abcam ab113476). Protein concentration was determined using the Pierce BCA assay. Samples were diluted into 1X NuPage LDS Sample Buffer (Invitrogen, NP0007), supplemented 1x sample reducing agent (Invitrogen, NP0004). 2.5 µg of native mixed histones and 625 ng of pure recombinant histone H3 were loaded on the gel.

12. Gene expression analysis and qRT-PCR

The nanoSTRING nCounter system was used for quantitatively analyzing gene expression using the Mouse Neuropathology panel of 760 mRNA probes. Total RNA was isolated from cultured mouse neurons treated with xcTauOs (250 nM total tau) or vehicle for 6 hours using the mirVana isolation kit (Invitrogen, AM1560). RNA integrity was evaluated by capillary electrophoresis using an Agilent Bioanalyzer. 100 ng of RNA with a RIN >7 was used per sample, and 3 biological replicates were used for each condition. Data analysis was done using the ROSALIND platform considering a p-value threshold of 0.05 for differential gene expression.

Semi quantitative real time PCR was used to quantify *MAPT* mRNA level in cultured mouse neurons after xcTauO or vehicle treatment for 6 hours. RNA was isolated using Trizol (Invitrogen, 15596026) and *MAPT* mRNA levels were quantified using One-Step qRT-PCR (Invitrogen, 11746100) in an Applied Biosystem StepOne Plus Real-Time PCR instrument as follows: 3 minutes at 50° C; 5 minutes at 95° C; 40 cycles of 15 seconds at 95 °C, 30 seconds at 60° C and 1 minute at 40° C; and 72° C to 90° C melting analysis. In all cases, *Actb* and *Rpl19* were used as reference genes, and 4 independent biological replicates with 2 technical replicates each were quantified. Primer sequences were obtained from Origene (MP208179, MP200232 and MP212857). Primer efficiency was calculated and incorporated in the ΔΔCt method analysis [110].

13. Statistical analysis

Data are presented as mean values of the number of independently conducted experiments indicated in the legend of each figure. Error bars represent the standard error of the mean (SEM). Statistical analysis was performed using Prism 9 software (GraphPad). Statistical tests used for all figures are indicated in the corresponding legends.

Results

1. Nuclear lamina invagination in human AD and transgenic mouse brains.

We first evaluated the morphology of neuronal nuclei in cortices from AD and age-mated cognitively normal individuals (Supplementary Table 1 shows clinical characterizations). Invaginated neuronal nuclei were identified by surrounding MAP2-positive cytoplasm and deep infoldings of the nuclear lamina, as determined by anti-lamin B1 immunofluorescence. ~70% of neuronal nuclei were invaginated in AD brains, whereas only ~30% showed such deformation in cognitively normal brains (Figure 1A). Quantitative western blotting of human prefrontal cortex detected 2 lamin B1 bands (Figure 1B), whose apparent molecular weights correspond to isoforms reported in the UniProtKB database, and the lamin B1 level in AD tissue was ~28% lower than in tissue from cognitively normal individuals.

We next studied nuclear morphology in 2 transgenic mouse lines: PS19, which overexpress human P301S tau, and accumulate tangles by 6 months and neuron loss within 9 months [111]; and CVN, which overexpress human APP with the Swedish, Dutch and Iowa mutations, are knocked out for nitric oxide synthase 2, and develop plaques, tangles and neuron loss within 12 months [112]. To ensure thorough neuroanatomical coverage, we sampled coronal sections from anterior, middle, and posterior brain regions for PS19 mice (Supplementary Figure 1), and lateral, middle, and medial sagittal sections from CVN mice (Supplementary Figure 2). Necab1, which is highly expressed only in layer IV neurons [113], was used to differentiate neurons in inner cortical layers to those in outer layers (Supplementary Figure 1A). Compared to age-matched WT mice, 6-month-old PS19 mice had higher levels of invaginated neuronal

nuclei, especially in deep cortical layers. Elevated levels of such nuclei were also found in deep cortical layers of lateral brain regions in CVN mice. Altogether, these findings indicate that invaginated neuronal nuclei are abundant *in vivo* in human AD brain, and in the brains of transgenic mouse models of AD and a pure tauopathy.

2. Human xcTauOs induce nuclear invagination and endogenous tau aggregates in cultured mouse neurons.

Previous studies established that pathogenically mutated intracellular tau can provoke neuronal nuclear deformation [1, 84], but possible roles for xcTauOs [114] in this process have not been reported. We therefore investigated effects of xcTauOs on neuronal nuclei. All 6 human CNS tau isoforms were expressed in bacteria and purified, (Supplementary Figure 3), and oligomerized by addition of arachidonic acid (ARA; Figure 2B) [107]. It should be noted that oligomers with apparent molecular weights of ~110-130 kDa and ~200 kDa on SDS gels are actually tau dimers and trimers, respectively, as determined by mass spectrometry [115]. Nuclear invagination was induced in neurons exposed to xcTauOs made from 2N4R tau or an equimolar mixture of all 6 isoforms, but not to tau monomer or vehicle controls (Figure 2). Compared to controls, xcTauOs increased the frequency of neuronal nuclear invagination by 63-95%. Dose-response and kinetic analyses established that xcTauOs made from 250nM total 2N4R tau caused maximum nuclear invagination within just 1 hour of treatment (Supplementary Figure 4). Because oligomers represented an average of ~30% of the total tau, and were mainly dimers and trimers, the total oligomer concentration that was maximally active was actually ~30 nM.

To evaluate the *in vivo* relevance of xcTauOs assembled from recombinant tau, we also prepared and tested soluble brain extracts from 21-month-old $hTau^{+/-}$ transgenic mice that express approximately equimolar levels of the 6 CNS tau isoforms encoded by human genomic tau DNA in the absence of full-length mouse tau [116]. Brain extracts from comparably aged littermates that were null for human tau ($hTau^{-/-}$) were used as controls. Western blots revealed that all $hTau^{+/-}$ brains contained detectable tau, but only some harbored TauOs, typically with a size range of ~100-160 kDa (Figure 3A). $hTau^{+/-}$ brain extracts containing TauOs and tau monomers, but not monomers alone, potently induced neuronal nuclear invagination (Figure 3A). The results described so far in this section indicate that xcTauOs made from recombinant tau can reliably substitute for TauOs made *in vivo* in brain, and that xcTauOs made from recombinant 2N4R tau are as effective as those made from a cocktail of all 6 recombinant CNS tau isoforms. Accordingly, all other experiments described in this report relied on xcTauOs made from recombinant 2N4R human tau.

In a prior study, we reported that xcTauOs made from recombinant human tau induce accumulation of intracellular tau aggregates in cultured mouse neurons, but we did not confirm the presence of endogenous mouse tau in those aggregates [117]. As shown in Figure 3B, conspicuous, perinuclear aggregates labeled with an antibody that recognizes mouse, but not human tau were abundant in xcTauO-treated cultured neurons.

3. The effect of xcTauOs on nuclear lamina architecture depends on intracellular tau.

A recent report [104] that intracellular TauOs causes translational stress prompted us to test whether the mouse tau aggregates that formed in cultured mouse neurons

exposed to human xcTauOs signal a requirement of intracellular tau for neuronal nucelar invagination induced by the xcTauOs. Accordingly, neurons derived from tau$^{-/-}$ mice [105] were exposed to xcTauOs. As shown in Figure 4, neuronal nuclei in tau$^{-/-}$ neurons did not invaginate after xcTau exposure, unless human (2N4R) tau was expressed in the cells by lentiviral transduction. We therefore conclude that the effects of xcTauOs on nuclear morphology depend on intracellular tau.

4. xcTauOs disrupt nucleocytoplasmic transport in cultured neurons.

The nuclear lamina provides a structural framework for nuclear pore complexes (NPCs), which regulate exchange of molecules larger than ~40 kDa globular proteins between the nucleus and the cytoplasm. Nucleocytoplasmic transport is negatively impacted by mutant lamins [118, 119], which prompted us to assess whether it is also functionally compromised by xcTauOs. We first tested this possibility by a dextran exclusion assay, in which digitonin-permeabilized cultured mouse neurons were exposed to fluorescein-tagged 70 kDa dextran. In this assay, NPCs that are structurally damaged allow greater penetration of the dextran-fluorescein into the nucleus than undamaged NPCs (Figure 5A). We found that xcTauOs caused ~36% more dextran-fluorescein to enter nuclei of neurons exposed to xcTauOs as compared to vehicle (Figure 5B).
Next, we assessed the effect of xcTauOs on active nucleocytoplasmic transport in live cultured mouse neurons by measuring the cytoplasmic/nuclear distribution of Ran, a small GTPase that reversibly shuttles between the nucleus and cytoplasm, but is normally highly enriched in nuclei at steady state [83, 120]. As shown in Figure 5C, xcTauOs caused an ~26% increase in the cytoplasmic/nuclear Ran ratio relative to a vehicle

control. Together, these dextran-fluorescein and Ran results demonstrate that xcTauOs functionally impair nucleocytoplasmic transport in neurons.

5. Differential gene expression caused by xcTauOs in cultured neurons.

Because the nuclear lamina serves as a tether for heterochromatin, we hypothesized that alterations of chromatin structure and gene expression accompanies the morphological distortion of neuronal nuclei caused by xcTauOs. To test that hypothesis, we first tested whether xcTauOs alter cultured mouse neuron levels of trimethylated lysine 9 of histone H3 (H3K9me3), which promotes transcriptional silencing. Supplementary Figure 5 shows that on western blots, the anti-H3K9me3 antibody used for these experiments was immunoreactive with bulk cell-derived histones, which include H3K9me3, but not with recombinant histone H3, which lacks post-translational modifications. This antibody also revealed by western blotting that the H3K9me3/total histone H3 ratio increased by ~52% after xcTauO exposure (Figure 6A).

Next, we investigated whether xcTauOs alter gene expression in cultured neurons using the nCounter platform from nanoSTRING for direct, unamplified measurement of 760 mRNAs associated with neuropathology. We found that for WT neurons, xcTauOs significantly altered mRNA levels for 15 genes, most of which were upregulated (Figure 6B). Annotation analysis of the differentially expressed genes highlights transcription functions based on genes like *Gtf2b*, *Srsf4*, *Prpf31* and *Cdk7*. In contrast, treatment of cultured tau$^{-/-}$ neurons with xcTauOs yielded a different pattern: more genes were down-regulated than up-regulated, and none of genes affected in WT neurons were affected in tau$^{-/-}$ neurons (Supplementary Figure 6). Interestingly, the most up-regulated gene in WT

neurons after xcTauO treatment was *MAPT*, which encodes tau (fold change = 3.93; Figure 6B). However, *MAPT* elevation did not reach significance threshold ($p < 0.20$), probably because of the high variation observed in this analysis. We therefore used an alternate method, qRT-PCR, to evaluate *MAPT* mRNA levels in WT neurons. That appproach detected a statistically significant 2.84-fold increase of *MAPT* mRNA after xcTauO treatment of WT neurons (Figure 6C).

Figure 1

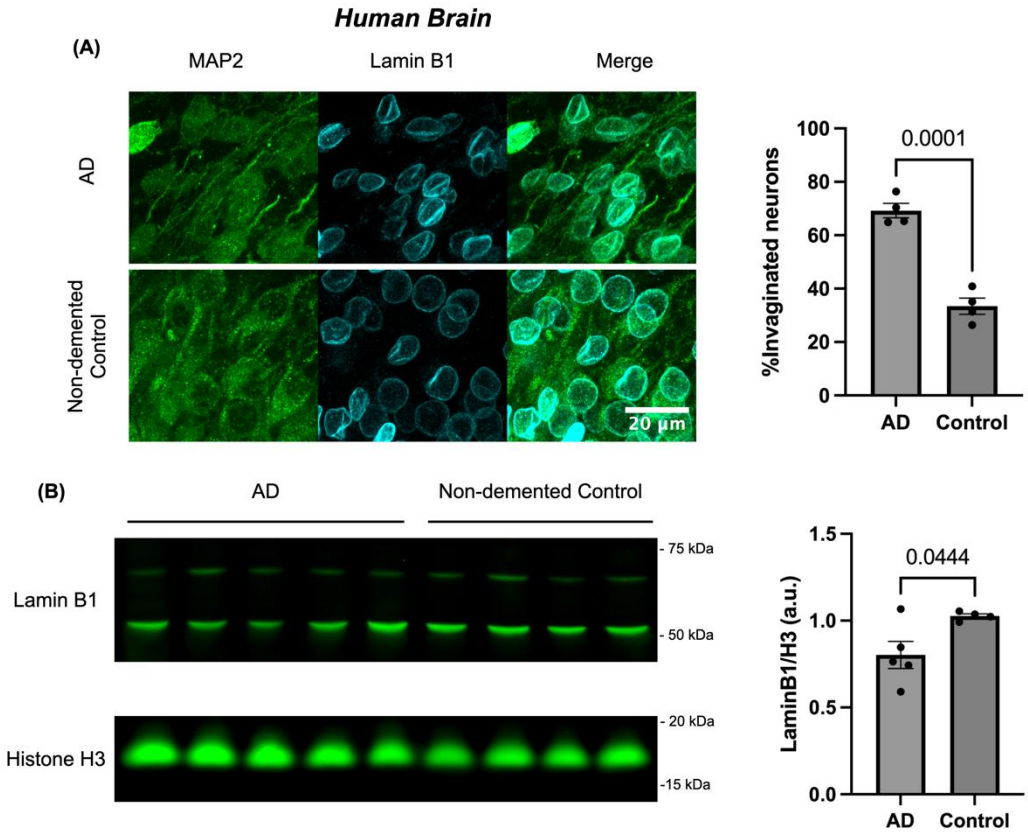

Figure 1 Lamina invaginations in neurons of the human AD cortex. (A) Incidence of neuronal lamina invaginations in vivo. Immunostaining of nuclear lamina (lamin B1, cyan) in neurons (MAP2, green) from human AD and non-demented control cortices. Significance was determined using unpaired t test; error bar represents SEM; n=4. (B) Representative western blot of lamin B1 in the prefrontal cortices of human AD and non-demented control brains. Lamin B1 signals were normalized against that of histone H3. The average lamin B1 to histone H3 ratio in non-demented control was arbitrarily defined as 1.0. Significance was determined using unpaired t test; error bar represents SEM; n=5 in AD group and n=4 in the control group.

Figure 2

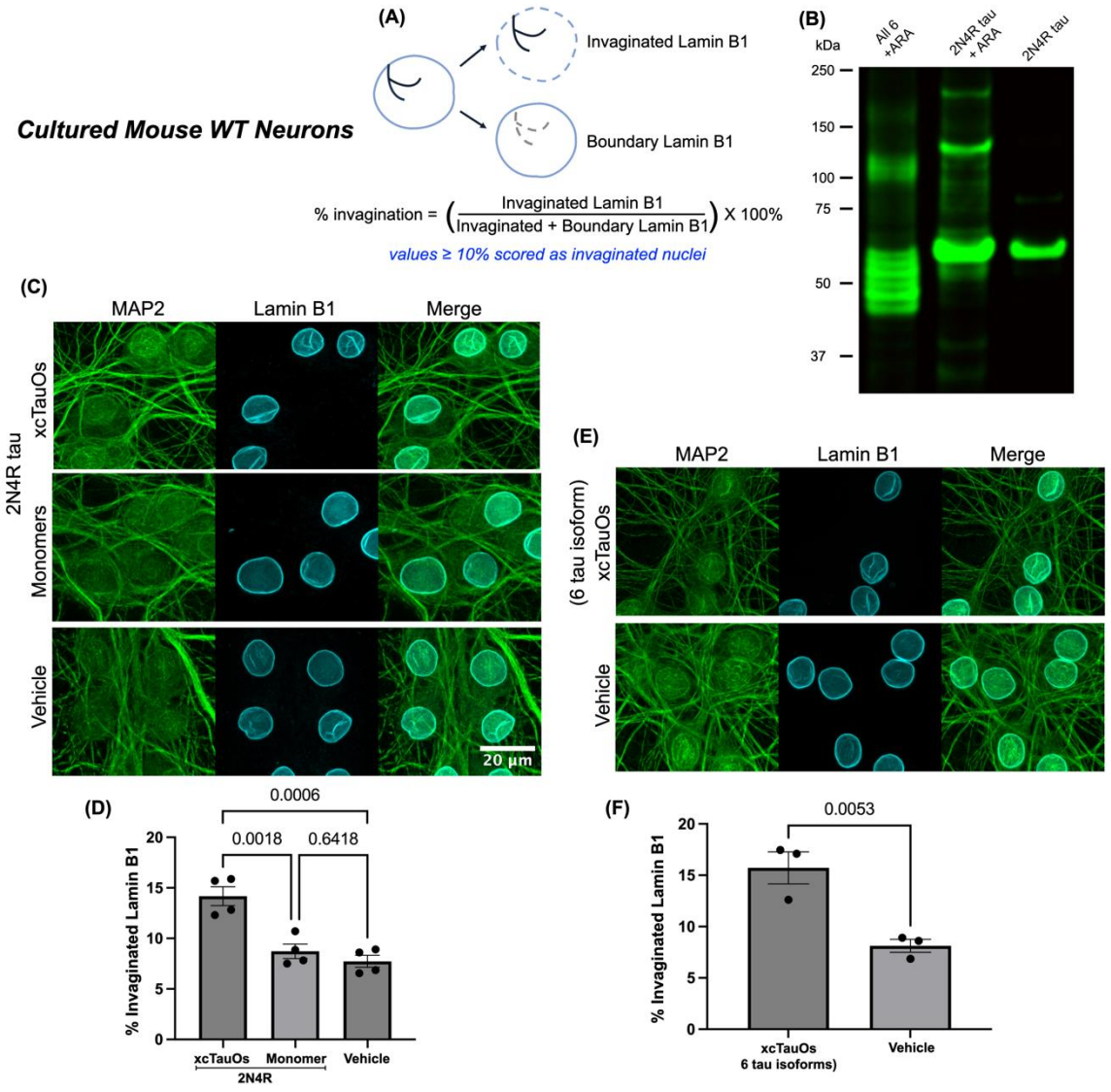

Figure 2 Extracellular oligomers (xsTauOs) induce lamina invagination in primary cultured neurons. (A) Schematic of image analysis strategy. lamin B1 staining was assigned as either the boundary or the invaginated. The deformation was measured as a ratio between the area of the invaginated lamin B1 over the total. (B) Characterization of tau oligomers. Western blot of oligomeric tau of mixed isoform composition (all 6 + ARA), oligomeric 2N4R tau (2N4R + ARA), and monomeric tau (2N4R) was probed with tau5 antibody. (C) Primary cortical neurons harboring lamina invagination after exposure to 250nM of xcTauOs for 1 hour. Immunostaining of nuclear lamina (lamin B1, cyan) in

neurons (MAP2, green). (D) Quantification of (C). Significance was determined using one-way ANOVA followed by Tukey's test; error bar represents SEM; n = 4 independent experiments. (E) Extracellular oligomers of mixed isoform composition cause nuclear invagination in primary cortical neurons. Cultures were exposed to 250nM of oligomer for 1 hour. Immunostaining of nuclear lamina (lamin B1, cyan) in neurons (MAP2, green). (F) Quantification of (E). Significance was determined using Student's t test; error bar represents SEM; n = 3 independent experiments.

Figure 3

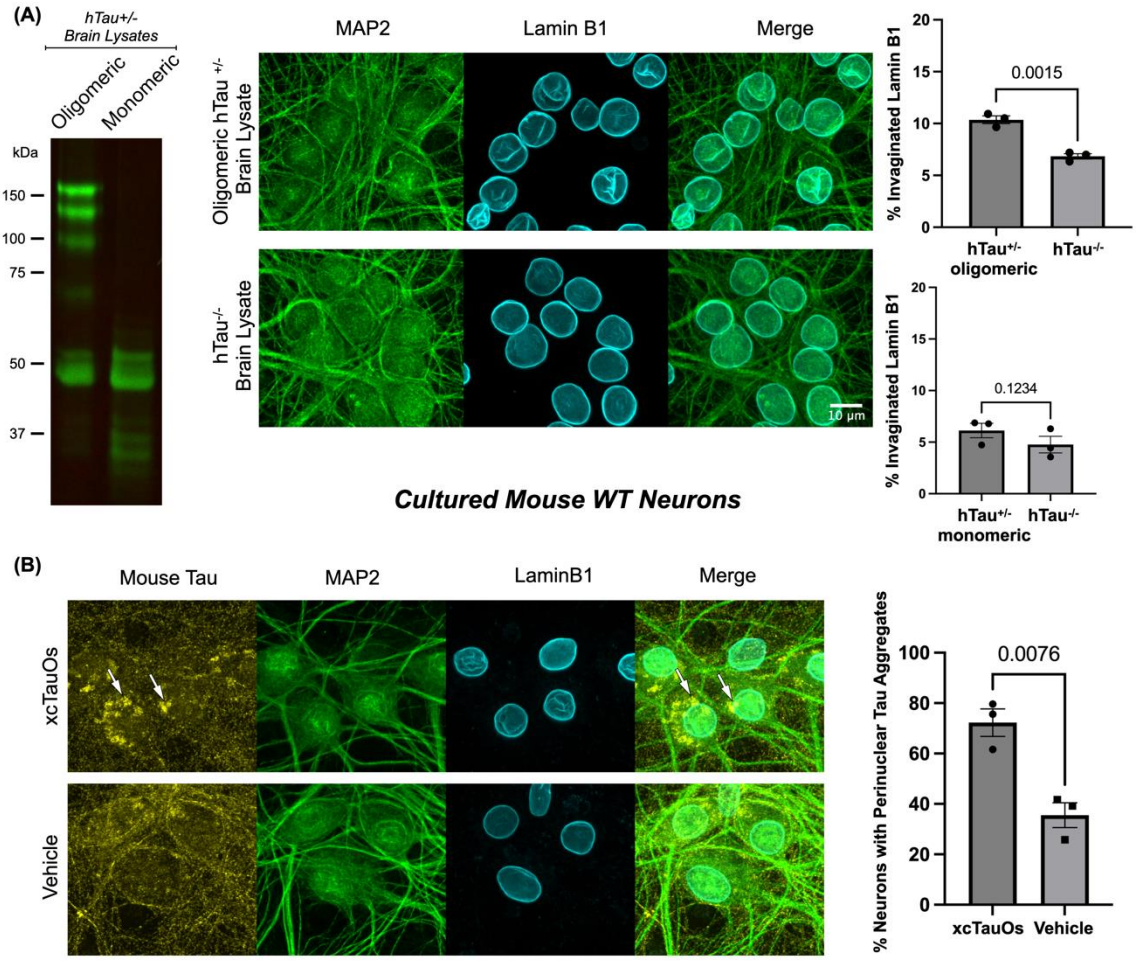

Figure 3 xcTauOs derived from hTau mouse brain induce lamina invagination in cultured neurons. (A) Characterization hTau$^{+/-}$ mouse brain-derived tau oligomers. Brain tissues were homogenized by sonication. Lysates were clarified by centrifugation and filtration. Western blot was probed with tau5 antibody. Primary cortical neurons harboring lamina invagination after exposure to hTau$^{+/-}$ mouse brain derived oligomeric or monomeric tau (0.7% v/v) for 4 hour. Immunostaining of nuclear lamina (lamin B1, cyan) in neurons (MAP2, green). Significance was determined using Student's t test; error bar represents SEM; n = 3 independent experiments. (B) Primary cortical neurons

harboring perinuclear tau aggregates after exposure to 250nM of xcTauOs for 1 hour. Immunostaining of nuclear lamina (lamin B1, cyan) and endogenous mouse tau (T49, yellow) in neurons (MAP2, green). Significance was determined using Student's t test; error bar represents SEM; n = 3 independent experiments.

Figure 4

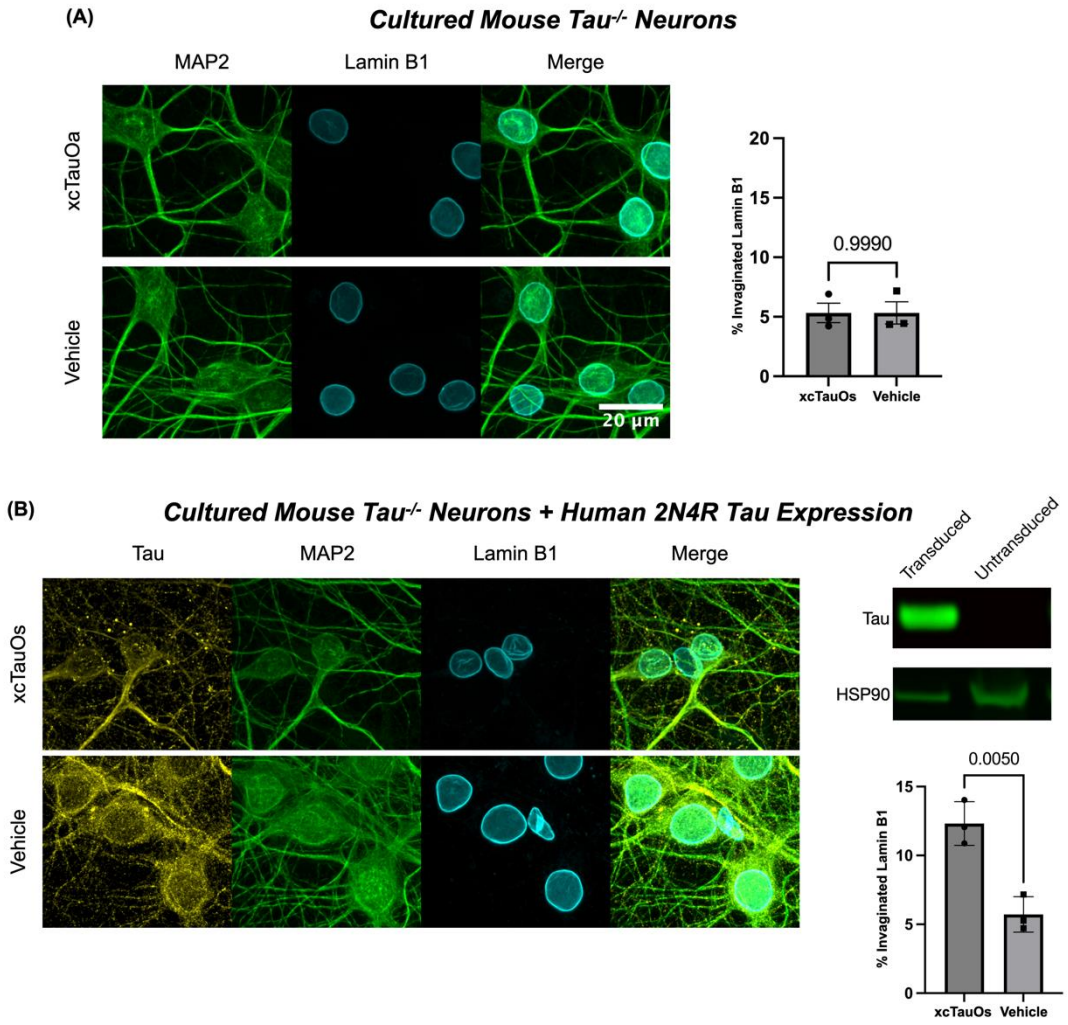

Figure 4 The effect of xcTauOs on nuclear structure depends on intracellular tau. (A) xcTauOs failed to induce lamina invagination in tau knock-out neurons. Cultures were treated with 250nM xcTauOs or vehicle for 1 hour. Immunostaining of nuclear lamina (lamin B1, cyan) in neurons (MAP2, green). Significance was determined using Student's t test; error bar represents SEM; n = 3 independent experiments. (B) Re-expression of 2N4R tau to tau knock-out neurons restores its sensitivity to xcTauOs. Cultures were treated with 250nM xcTauOs or vehicle for 1 hour. Lentiviral transduction was done 3 days prior to treatment. The expression of tau was confirmed by immunostaining with an

antibody against total tau, tau5 (yellow) and western blot. Only cells positive for MAP2 and tau staining were included in the analysis. Significance was determined using Student's t test; error bar represents SEM; n = 3 independent experiments.

Figure 5

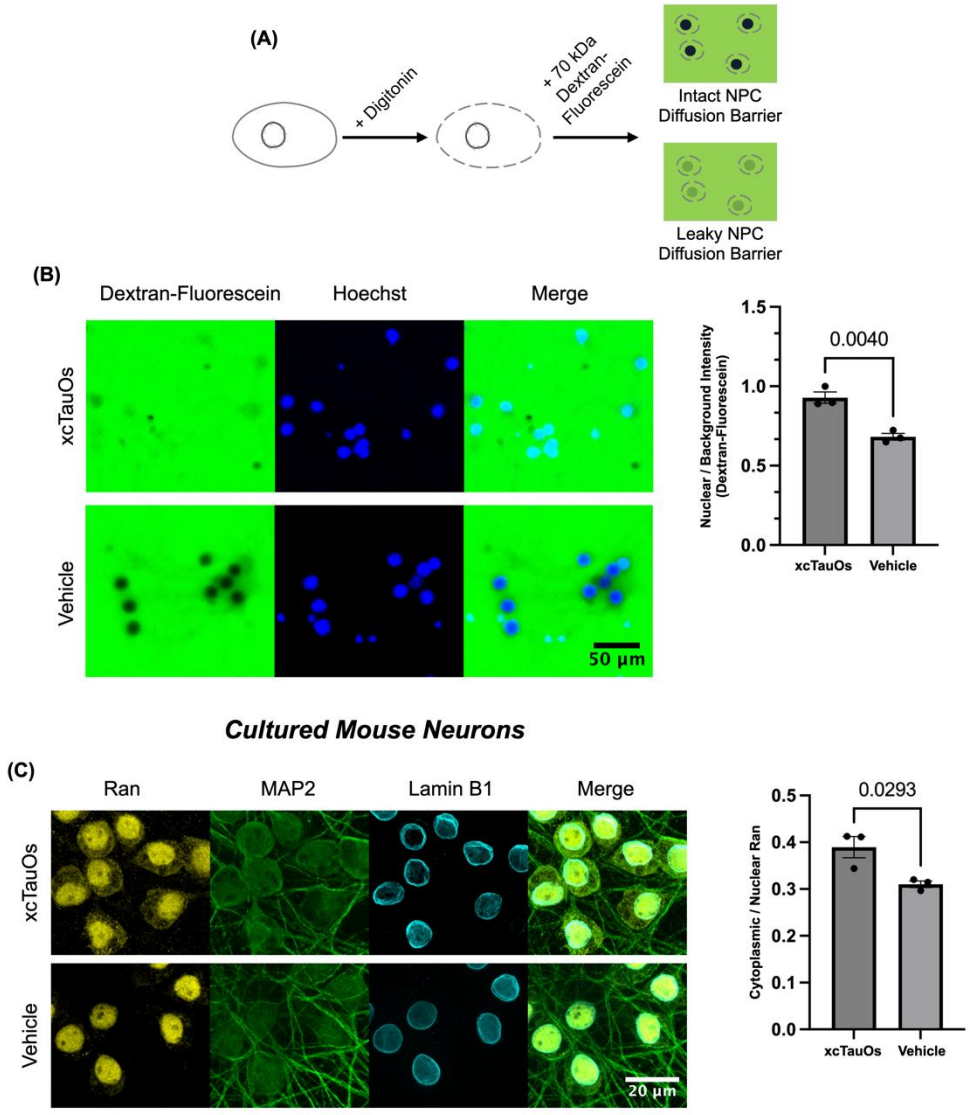

Figure 5 xcTauOs disrupt nucleocytoplasmic transport in cultured neurons. (A) Schematic illustration of dextran exclusion assay. Neurons were treated with digitonin to permeabilize the plasma membrane and incubated with fluorescein labeled dextran (70 kDa). (B) Neurons treated with xcTauOs had leaky NPC diffusion barrier. Cultures were treated 250nM xcTauOs or vehicle for 24hrs and subjected to dextran exclusion assay. The nuclei were identified by counterstaining with Hoechst 33342. All image illustrated single focal plane. The leakiness was measured as a ratio between the mean pixel intensity of intranuclear fluorescent signal over extranuclear signal. Significance was determined using

Student's t test; error bar represents SEM; n = 3 independent experiments. (C) Ran mislocalization in neurons exposed xcTauOs. Cultures were treated 250nM xcTauOs or vehicle for 24hrs and immunostained for Ran (yellow), MAP2 (green) and lamin B1 (cyan). Ran mislocalization was measured as a ratio between the mean pixel intensity of cytoplasmic Ran signal over nuclear signal. Significance was determined using Student's t test; error bar represents SEM; n = 3 independent experiments.

Figure 6

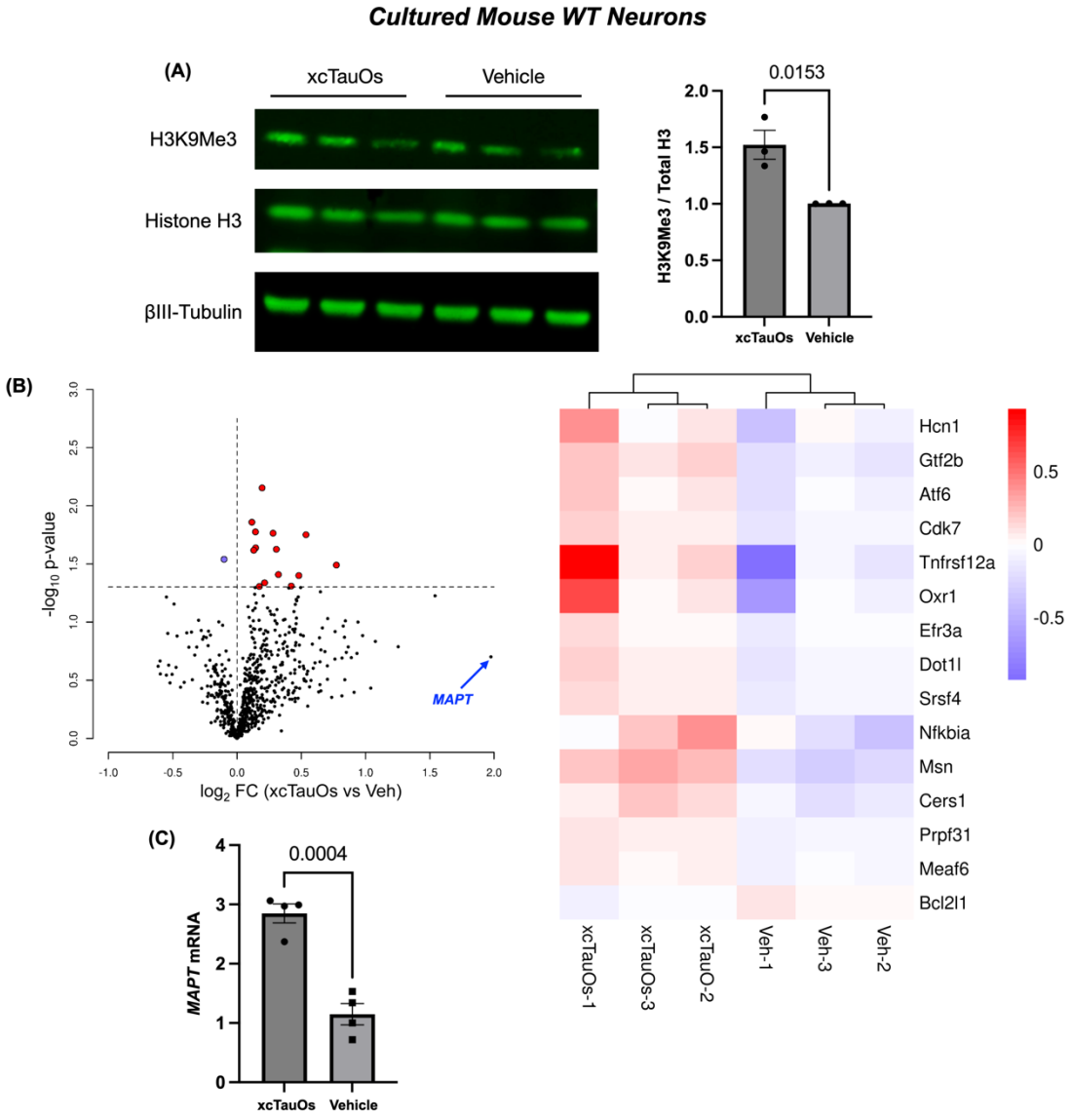

Figure 6 Differential gene expression caused by xcTauOs in cultured neurons. (A) Representative western blot of H3K9Me3. Primary cultures were treated 250nM xcTauOs or vehicle for 24hrs. H3K9Me3 signals were normalized against that of histone H3. The average H3K9Me3 to histone H3 ratio in control groups was arbitrarily defined as 1.0. Significance was determined using unpaired t test; error bar represents SEM; n=3 independent experiments. (B) Volcano plot and heatmap showing the comparison between gene expression levels. Primary cultures were treated 250nM xcTauOs or vehicle for 6hrs. Differentially expressed genes are shown in color (blue, down-regulated; red, up-regulated).

n=3 independent experiments. (C) Relative quantification by qRT-PCR of *Mapt* mRNA levels in primary cultures treated with 250nM xcTauOs or vehicle for 6hrs. ΔΔCt method was used and the average fold change relative to control group, arbitrarily defined as 1.0, is shown. Significance was determined using unpaired t test; error bar represents SEM; n=4 independent experiments.

Supplementary figure 1

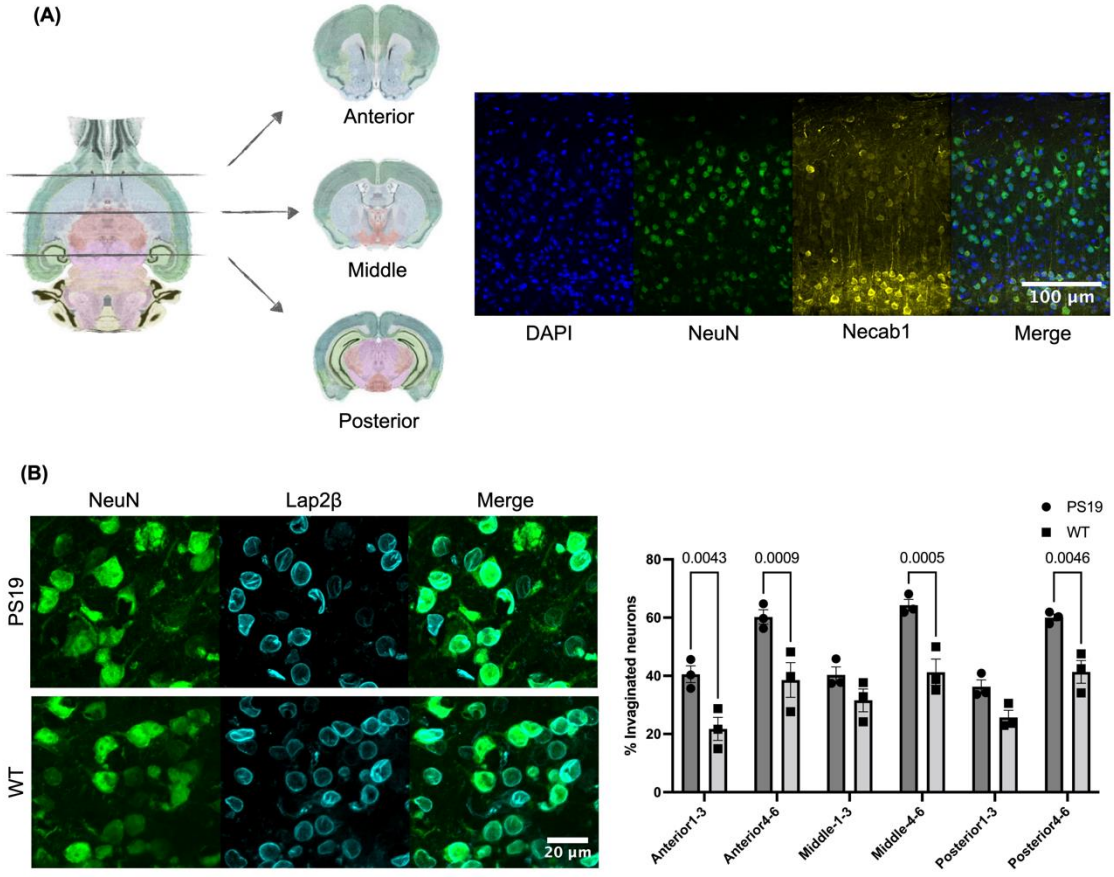

Supplementary figure 1 Lamina invaginations in PS19 mice. (A) Schematic of sample collection. To ensure thorough neuroanatomical coverage, coronal sections from anterior, middle, and posterior brain regions are selected based on their distinctive morphologies. Image credit: Allen Institute for Brain Science. [https://mouse.brain-map.org/agea] Superficial and deep cortical layers were identified by the immunostaining of Necab1 (yellow), a maker for neurons (NeuN, green) from cortical layer IV. (B) Incidence of neuronal nuclear invaginations in the deep cortical layers from 6-mo PS19 mouse brain. Immunostaining of nuclear lamina (LAP2β, cyan) in neurons (NeuN, green). Significance was determined using two-way ANOVA followed by Bonferroni's test; error bar represents SEM; n=3.

Supplementary figure 2

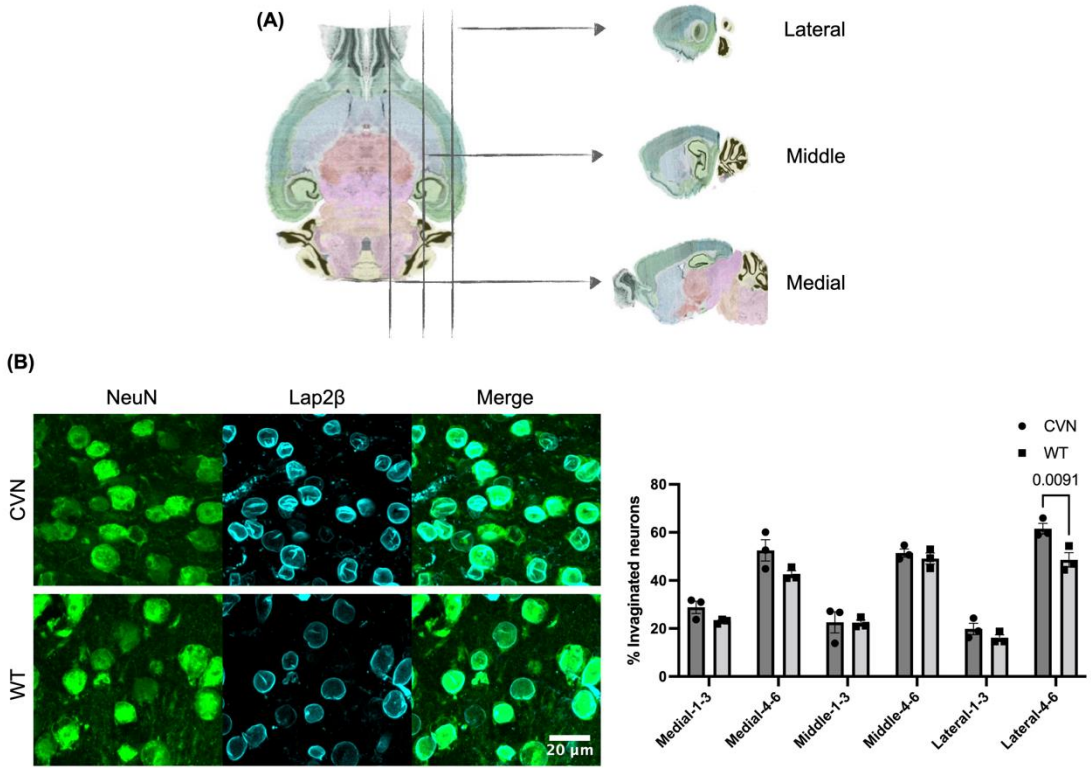

Supplementary figure 2 Nuclear lamina invaginations in CVN mice. (A) Schematic of sample collection. To ensure thorough neuroanatomical coverage, sagittal sections from lateral, middle, and medial brain regions are selected based on its distinctive morphology. (B) Incidence of neuronal nuclear invaginations in the deep cortical layers from 22-mo CVN mouse brain. Immunostaining of nuclear lamina (LAP2β, cyan) in neurons (NeuN, green). Significance was determined using two-way ANOVA followed by Bonferroni's multiple correction test; error bar represents SEM; n=3.

Supplementary figure 3

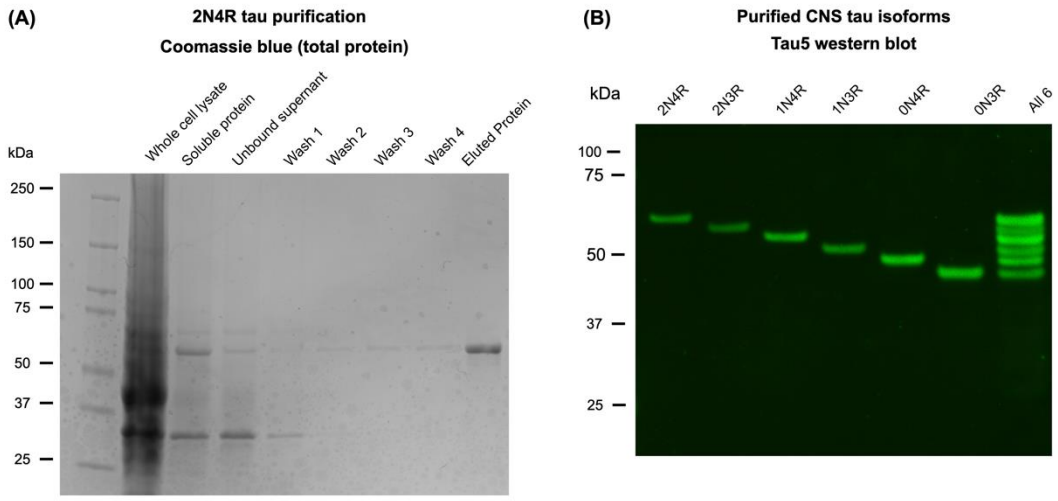

Supplementary figure 3 Recombinant tau proteins used in this study. (A) Validation of recombinant 2N4R tau purification. Samples taken along the course of purification were run on the SDS-PAGE gel and stained with Coomassie blue. Bacterial cells were lysed by sonication (lane 2, whole cell lysate). After clarified by centrifugation (lane 3, soluble protein), lysate was incubated with metal affinity resin. The supernatant was then removed (lane 4, unbound protein) and the beads were washed 4 times (lanes 5-8). The final protein was eluted and collected (lane 9, eluted protein). (B) Recombinant tau isoforms used in this study. Western blot was probed with total tau antibody, tau5.

Supplementary figure 4

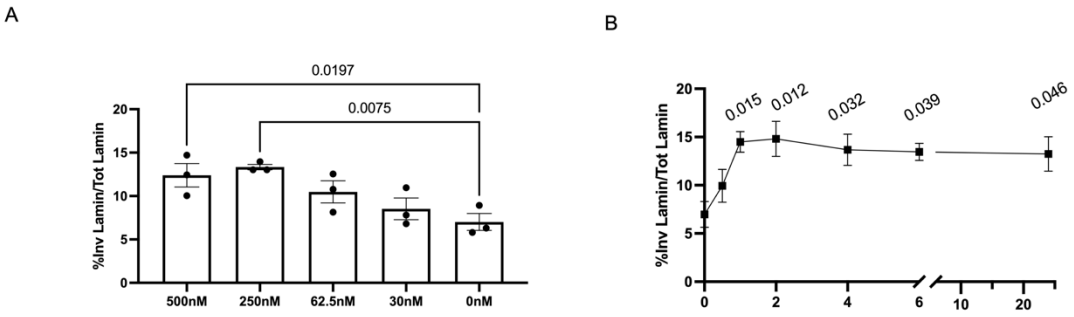

Supplementary figure 4 Dose response and time course impacts of xcTauOs on neuronal nuclear structure. (A) Dose response impact of xcTauOs on neuronal nuclear structure. Primary cortical cultures were exposed to various concentration of xcTauOs for one hour. Significance was determined using one-way ANOVA followed by Dunnett's test; error bar represents SEM; n = 3 independent experiments (1-2 technical replicates, at least 50 neurons were counted in each replicate). (B) xcTauOs cause rapid, long lasting lamina invagination in cultured neurons. Primary cortical cultures were exposed to 250nM of xcTauOs and harvested at various time points. Significance was determined using one-way ANOVA followed by Dunnett's test; error bar represents SEM; n = 3 independent experiments (2 technical replicates, at least 50 neurons were counted in each replicate).

Supplementary figure 5

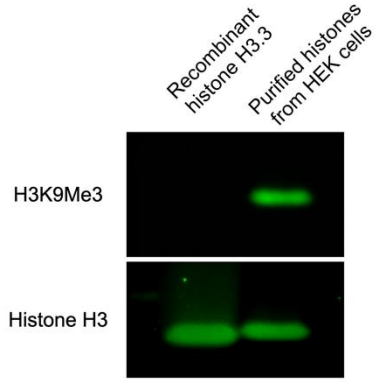

Supplementary figure 5 Validation of H3K9Me3 antibody**.** Western blot analysis of unmodified recombinant histone and native histones (bearing a full repertoire of post-translational modifications) extracted from HEK cells.

Supplementary figure 6

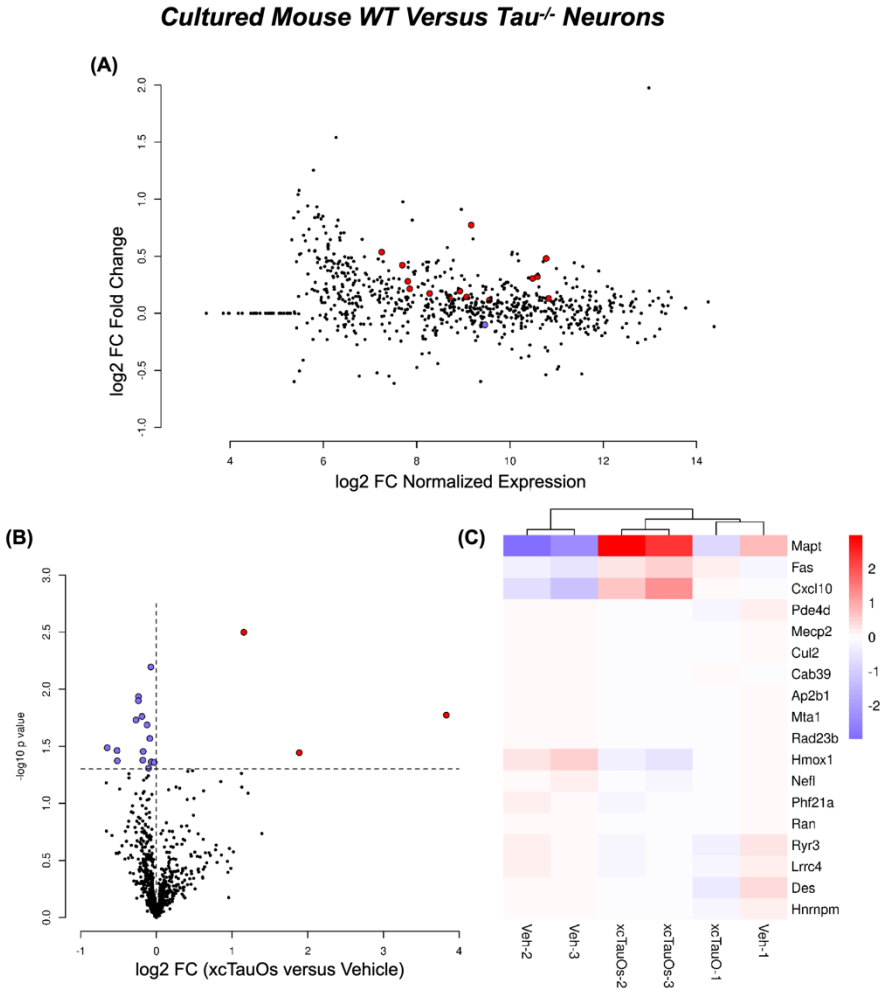

Supplementary figure 6 Differential gene expression caused by xcTauOs exposure in wild type and tau knock-out neurons evidenced by nCounter. (A) The MA plot shows the relationship between expression and fold-change in the comparison between xcTauOs-treated and vehicle-treated wild-type neurons (see Figure 6C). (B) Volcano plot for the comparison between xcTauOs-treated and vehicle-treated tau knock-out neurons. Differentially expressed genes are shown in color (blue, down-regulated; red, up-regulated). (C) Heatmap showing gene expression levels of differentially expressed genes indicated in (B).

Supplementary Table 1. Patient Demographics and Tissue Specifics (staining and western blotting).

Sample identification	Group	Age	Sex	PMI (hr)	Western blot	Staining
223	AD	69	F	11.5	√	
241	AD	73	F	9.5	√	
156	AD	77	F	4.5	√	
178	AD	77	F	4.5	√	
127	AD	79	M	6	√	
A10-212	AD	93	F	NA		√
A15-167	AD	88	F	NA		√
A13-66	AD	89	M	NA		√
A16-26	AD	75	M	NA		√
228	Control	64	F	17	√	
191	Control	70	F	9	√	
216	Control	87	F	13	√	
213	Control	61	M	6	√	
A14-34	Control	81	F	NA		√
A14-35	Control	73	M	NA		√
A16-205	Control	84	F	NA		√
A16-236	Control	84	F	NA		√

Supplementary table 2. Primary and Secondary Antibodies

Name	Tag	Source; Cat #
chicken anti-MAP2	None	abcam; ab92434
mouse anti-pan-tau (Tau5)	None	Dr. Lester (Skip) Binder (deceased)
Mouse anti-mouse-tau(T49)	None	Sigma-Aldrich; MABN827
mouse anti-NeuN	None	Millipore; MAB377
mouse anti-βIII-tubulin	None	Dr. Tony Spano
mouse anti-H3K9me3	None	Novus Biologicals; NBP1-30141
mouse anti-Ran	None	BD Biosciences; 610341
mouse anti-Lap2β	None	BD Biosciences; 611000
mouse anti-tau (T49)	None	Millipore; MABN827
rabbit anti-LaminB1	None	abcam; ab16048
rabbit anti-H3	None	Cell Signaling Technology; #9715
rabbit anti-Necab1	None	Sigma-Aldrich; HPA023629
rabbit anti-HSP90	None	Cell Signaling Technology; C45G5
goat anti-mouse IgG	Alexa Fluor 488	Invitrogen; A-11001
goat anti-chicken IgY	Alexa Fluor 568	Invitrogen; A-11041
goat anti-rabbit IgG	Alexa Fluor 647	Invitrogen; A-21244
goat anti-rabbit IgG	IRDye 680RD	LI-COR; 926-68071
goat anti-mouse IgG	IRDye 800CW	LI-COR; 926-32210

Chapter 3
Discussion and future directions

Discussion

Accumulating evidence has demonstrated that tau is released into the extracellular space independent of cell death and the release is enhanced by neuronal activity [121]. Much effort has been focused on the mechanisms of trans-synaptic propagation of pathological tau. However, the pathophysiological function of extracellular tau and related pathways underlying cellular dysfunction remain to be elucidated.

Our study provides several lines of evidence that xcTauOs induce nuclear lamina invagination in cultured primary neurons. We utilize arachidonic acid to induce oligomerization of recombinant tau [107]. On the western blot, the apparent molecular weight of these oligomers is similar to that found in AD human brain [115]. Moreover, an antibody raised against ARA-induced oligomers also selectively labels pretangles in human AD brain tissue sections [115, 122]. We also obtained tau oligomers from hTau mouse brains, which express only human tau and accumulate aggregated, hyperphosphorylated tau from 9 months of age. We demonstrated that xcTauOs of 2N4R, xcTauOs of mixed conformations, and xcTauOs derived from hTau brains are equally potent in challenging neuronal nuclei integrity.

Furthermore, this effect is contingent on intracellular tau. We observed that xcTauOs failed to induce lamina invagination in tau knock out neurons, yet re-expression of human 2N4R tau restored their sensitivity to xcTauOs. The mechanism by which xcTauOs distort nuclear membrane through intracellular tau is unclear. We observed that endogenous tau formed large, bright speckles in the perinuclear region upon xcTauOs exposure. This is in accordance with a previous study, which demonstrated that the presence of tau oligomers in the extracellular space leads to a redistribution of

intracellular tau into the somatodendritic compartment [117]. In healthy neurons, tau primarily resides in the axon and interacts with microtubule, thereby stabilizing microtubule and regulating axonal transport [123]. Therefore, it is likely that xcTauOs-induced tau mislocalization changes microtubule dynamics, particularly in the perinuclear region. Indeed, lamina invagination reflects decreased membrane tension, indicating improper cytoskeletal/nucleoskeletal coupling at the interface of the nuclear membrane [124]. Additionally, recent research shows that xcTauOs are endocytosed into neurons through low-density lipoprotein receptor-related protein 1 (LRP1) within an hour. Therefore, tau oligomer uptake is also a likely event in our experiment condition [125].

The deterioration of nuclear architecture and dysfunction of nuclear membrane are common characteristics of cellular aging, as well as hallmarks of several diseases, including Hutchinson-Gilford syndrome, some types of cancer and neurodegeneration [126-128]. In this study, we confirmed the presence of nuclear invagination in the post-mortem AD brain, consistent with previous works [1, 81]. Moreover, nuclear contour irregularity in AD is accentuated by nucleoporin immunohistochemistry (key building blocks of NPC), often in juxtaposition to neurofibrillary tangles [81]. Recent findings have also reported that pathological tau directly interacts with nucleoporin, resulting in defective nucleocytoplasmic transport [83, 84]. We observed functional impairment of NPC in primary neurons exposed to xcTauOs. There is a clear change to the diffusion barrier maintained by NPCs at the nuclear membrane, evident by *in vitro* analysis of pore permeability with fluorescence tagged inert dextran molecules. Active protein import and export are altered as well, reflected by Ran distribution, an endogenous protein whose subcellular localization is essential for regulated cargo shuttling. These results have

profound implications. For example, BRCA1, one of the key players in DNA damage response pathways, is sequestered into cytoplasm in post-mortem AD, PSP and FTD brains [129]. Proteins related to RNA processing, including Musashi and RNA polymerase II subunit RPB1, has also been shown to mislocalize from the nucleus to the cytoplasm of neurons in AD [70, 130]. Our evidence suggests that mislocalization of these proteins may be a consequence of tau-mediated nucleocytoplasmic transport disruption in AD and related tauopathies.

To assess nucleocytoplasmic transport, we exclusively used cultured neurons in our experiments. While a prior study suggested that the diffusion barriers of nuclei isolated from human AD brains are leaky [83], there is currently no evidence of disrupted active nucleocytoplasmic transport. Immunohistochemical staining of Ran in the brains of individuals with AD and other tauopathies will provide *in vivo* evidence for our findings.

Additionally, nuclear lamina serves as a platform for the organization of repressive elements in the nucleus, where heterochromatins directly interact with and thereby are tethered to lamins and lamin associated protein. We speculate that nuclear lamina deformation also disrupts chromatin organization and overall transcription profile. Indeed, we found an elevation of H3K9Me3 level, an epigenetic modification associated with heterochromatin, in primary cultures exposed to xcTauOs. This is in concordance with previous report that H3K9me3-dependent heterochromatin condensation is robustly elevated in the end-stage sporadic AD post-mortem temporal cortices [93]. However, another study has reported a widespread loss of H3K9me2 in the brains of *Drosophila* expressing pathogenic tau [1]. Since H3K9me2 and H3K9me3 decorate different

genomic regions [131], these results are in fact complementary to each other. Here we only focused on H3K9Me3 via western blot. Characterization of additional markers for heterochromatin, such as H3K9me2, H3K27me3, and HP1α, using both western blot and immunocytochemistry, will provide a much more comprehensive visualization of the neuronal chromatin state in our experimental model.

Lastly, we demonstrated that nuclear invagination caused by xcTauOs leads to downstream effect on genome transcription. We explored fluctuation in mRNAs levels using the nCounter platform with the neuropathology panel. mRNA abundance for 760 genes were directly quantified in wild type and tau knock-out neurons exposed to xcTauOs or vehicle. Differential gene expression analysis revealed mostly up-regulation events after 6 hours of treatment with xcTauOs in wild-type neurons. Several of those up-regulated genes were associated to transcription and splicing annotations, such as general transcription factor IIB, Ser/Arg-splicing factor 4 and cyclin dependent kinase 7. This result was not reproducible in tau knock-out neurons. Concordantly, neither of the transcription-related genes altered in wild-type neurons was deregulated in tau knock-out.

One particularly interesting hit is activating transcription factor 6 (ATF6), which is one of the three stress sensors that trigger the unfolded protein response (UPR). When the protein folding machinery in the ER lumen are overwhelmed, UPR is activated as a protective response to ER stress. A transmembrane protein, ATF6 is cleaved under stress and the resulting N-terminal fragment relocates to the nucleus and activates the transcription of more genes responsive to UPR. While ER stress has been documented in postmortem AD brain samples, the exact mechanism liking UPR to AD remains elusive. In a *C-elegance* model of tauopathy, *atf6* loss of function exacerbates behavior defects

[132]. Further research is necessary to fully elucidate how ATF6 and UPR interact with pathological tau and contribute to AD manifestation.

It is worth noting that, in the nCounter analysis, the fold change values are not particularly high. For example, in the comparison between xcTauOs and vehicle treated wild type neurons, up-regulated genes show an average increase of 25%. However, as observed in the MA plot (Figure S7A), the mean expression level of differentially expressed genes is high. This indicates that, despite the increase is not dramatically high in fold terms, the actual expression level is up regulated. Several reasons could explain this observation. First, high variability was observed among samples (batch effects were considered in the analysis), partly due to the heterogeneity of the cell populations. Our primary cultures consist of both neurons and glial cells, and we have yet to investigate how glial cells respond to xcTauOs. Additionally, the culture was only exposed to xcTauOs for 6 hours, during which we detected an immediate early response. However, if the exposure time were extended to 24 or 48 hours, we would expect to observe a higher level of fold changes accumulating. Lastly, the turn-over rate of individual mRNA may respond to xcTauOs differently. Therefore, further studies are needed to confirm the up regulation of individual genes, particularly at the protein level.

In conclusion, our results imply an unconventional pathway underlying tau-induced neuropathology. xcTauOs are likely triggers of nuclear membrane deformation and associated impairments of nuclear biology observed in neurodegenerative diseases.

Future Directions

The results presented in this thesis can be expanded upon in multiple ways to further elucidate the connections among tau pathology, nuclear invagination, and neuronal dysfunction in AD. Although this thesis demonstrated the necessity of endogenous tau in xcTauOs-induced lamina invagination, the exact mechanism underlying this morphological change remains elusive. Preliminary results indicate that within an hour of exposure to xcTauOs, endogenous tau began to form bright speckles in the perinuclear region. There are two possible explanations, and they are not mutually exclusive: mislocalization of pre-existing endogenous tau protein or de novo protein synthesis. Pretreatment with cycloheximide, a small molecule that inhibits translational elongation and protein synthesis, would demonstrate whether xcTauOs induce endogenous tau protein synthesis. The presence of tau in the somatodendritic compartment might impact the neuronal microtubule dynamics. To test this hypothesis, live imaging of neurons transduced with GFP-tagged EB3, the microtubule plus-end binding protein, would provide valuable insight into whether actively growing microtubules exert improper force on the nuclear membrane.

Furthermore, it would be of great interest to determine whether endogenous tau in the perinuclear region is hyperphosphorylated. Previous research has shown that pseudophosphorylated tau (S199E, T212E, T231E, and S262E) disrupts the nuclear lamina of transiently transfected HEK-293 cells [63]. These phosphorylation sites serve as a good starting point for further investigation. Phosphospecific antibodies should be first validated on the western blot with alkaline phosphatase. Immunostaining on fixed neurons exposed to xcTauOs can then determine the subcellular localization of

endogenous that becomes hyperphosphorylated, if there is any. Subsequent lentiviral transduction of phosphomimetic tau can be used to demonstrate whether tau hyperphosphorylation alone is sufficient for neuronal lamina invagination.

Another follow-up question is whether tau uptake plays a role in xcTauOs-induced lamina invagination. Evidence suggests that upon internalization, misfolded tau acts as a seed that induces conformational changes in normal tau, promoting oligomer and fibril formation. Aggregated tau has been clearly shown to efficiently enter neurons through heparan sulfate proteoglycans (HSPGs), LRP-1, and dynamin-dependent endocytosis [125, 133, 134]. To test this hypothesis, primary neuron cultures could be treated with various agents against tau internalization and screened for lamina invagination and endogenous tau mislocalization. For example, LRP1 can be knocked down by antisense shRNA. This experiment can be complemented by co-treatment with LRP1-binding protein, receptor-associated protein (RAP), as a competing ligand for xcTauOs.

What's more, histological analysis has revealed that the majority of invaginated neurons are located in deep cortical layers. In fact, regardless of the mouse genotype, cortical layer I had the lowest frequency of neuronal invagination. This layer is also devoid of excitatory neurons. Therefore, it is worth investigating whether xcTauOs selectively impair excitatory neurons. The cell identity in primary cultures can be easily identified by immunostaining with glutamatergic neuron markers, such as vesicular glutamate transporters 1 (vGlut1). An initial experiment would be a careful match of the lamina invagination to the excitatory or inhibitory nature of the neuron via immunofluorescence. A previous study has demonstrated that stimulation of synaptic

NMDA receptors, one of the ionotropic receptors to glutamate, leads to nuclear invagination in cultured rat hippocampal neurons. This process depends on calcium entry and the ERK-MAP signaling pathway [135]. Therefore, we can next investigate whether xcTauOs lead to calcium influx via calcium imaging. Genetically encoded calcium sensors, such as GCaMP-X, are great tools for this purpose [136]. Additional tags of NES and NLS motifs should be appended to the reporter sequence for specific subcellular localization, which allows us to visualize whether xcTauOs alter cytoplasmic and/or nuclear calcium dynamics and their respective time frames.

Additionally, intracellular calcium concentration change might be a downstream consequence of lamina invaginations. Research in this thesis shows that lamina invagination interferes with several key aspects of nuclear biology, including nucleocytoplasmic transport, chromatin organization, and DNA transcription. The outer membrane of the nuclear envelope is continuous with ER and the shared luminal space is a major storage site for intracellular calcium, which plays an important role in gene expression regulation. Previous research showed that *in vivo* expression of human R406W tau, which leads to lamina invagination, also causes a depletion of nuclear calcium in Drosophila [137]. Therefore, it is conceivable that the architectural change of nuclear envelope leads to a change in intracellular calcium dynamics. Given the limited identification of surface binding partners to xcTauOs that would lead to intracellular calcium rise, pre-incubation with BAPT-AM, a non-selective membrane permeant calcium chelator, will validate whether calcium is involved in the mechanisms underlying xcTauO-induced lamina invagination.

Another promising direction for further investigation is the characterization of chromatin organization in neurons exposed to xcTauOs. The limited scope of this study, which only focused on H3K9Me3 (an epigenetic marker for heterochromatin) via western blot, was due to difficulties in validating antibodies against specific epigenetic modifications. It would be interesting to study other markers for heterochromatin, such as H3K9me2, H3K27me3, and HP1α, using both western blot and immunocytochemistry. This characterization can also be extended into human and mouse brain tissues. Furthermore, chromatin tracing could provide a much more detailed view of chromatin organization at a single-cell resolution. This is a DNA FISH-based sequential imaging and reconstruction procedure that allows visualization of chromatin folding at both chromosome and genome scales [138, 139].

The next proposed experiment is currently in progress. The nCounter analysis has demonstrated that exposure to xcTauOs leads to differential gene expression in cultured primary neurons. The neuropathology panel provided by NanoSTRING has allowed us to quantify the gene expression levels of 760 genes. Annotation analysis of differentially expressed genes has highlighted transcription functions based on genes such as Gtf2b, Srsf4, Prpf31, and Cdk7. These results prompted us to perform total RNA sequencing (RNA-seq), which will provide a comprehensive picture of the impact of xcTauOs on the whole transcriptome, especially genes that give rise to functional non-coding RNAs. Several non-coding RNAs, including microRNAs (miR-132 and miR-129), long intergenic non-coding RNA (lincRNA), and piwi-interacting RNAs, have been associated with AD pathogenesis [81, 120]. Non-coding RNAs carry out diverse functions in normal physiology and pathology. In the context of AD, different miRNAs are associated with

either amyloid plaques or NFT, indicating that they impact disease progression through different pathogenic pathways [120]. RNA-seq will identify if any non-coding RNA has been impacted by xcTauOs, whose presence features early-stage AD. Overall, RNA-seq will identify novel targets in our experimental model and expand the directions we could pursue.

Reference

1. Frost, B., F.H. Bardai, and M.B. Feany, *Lamin Dysfunction Mediates Neurodegeneration in Tauopathies.* Curr Biol, 2016. **26**(1): p. 129-36.
2. Weingarten, M.D., et al., *A protein factor essential for microtubule assembly.* Proc Natl Acad Sci U S A, 1975. **72**(5): p. 1858-62.
3. Association, A.s., *2022 Alzheimer's disease facts and figures.* Alzheimers Dement, 2022. **18**(4): p. 700-789.
4. McKhann, G.M., et al., *The diagnosis of dementia due to Alzheimer's disease: recommendations from the National Institute on Aging-Alzheimer's Association workgroups on diagnostic guidelines for Alzheimer's disease.* Alzheimers Dement, 2011. **7**(3): p. 263-9.
5. Hansson, O., et al., *Advantages and disadvantages of the use of the CSF Amyloid beta (Abeta) 42/40 ratio in the diagnosis of Alzheimer's Disease.* Alzheimers Res Ther, 2019. **11**(1): p. 34.
6. Alexander, G.E., et al., *Longitudinal PET Evaluation of Cerebral Metabolic Decline in Dementia: A Potential Outcome Measure in Alzheimer's Disease Treatment Studies.* Am J Psychiatry, 2002. **159**(5): p. 738-45.
7. Mielke, M.M., et al., *Plasma phospho-tau181 increases with Alzheimer's disease clinical severity and is associated with tau- and amyloid-positron emission tomography.* Alzheimers Dement, 2018. **14**(8): p. 989-997.
8. Thijssen, E.H., et al., *Diagnostic value of plasma phosphorylated tau181 in Alzheimer's disease and frontotemporal lobar degeneration.* Nat Med, 2020. **26**(3): p. 387-397.
9. Mila-Aloma, M., et al., *Plasma p-tau231 and p-tau217 as state markers of amyloid-beta pathology in preclinical Alzheimer's disease.* Nat Med, 2022. **28**(9): p. 1797-1801.
10. Janelidze, S., et al., *Cerebrospinal fluid p-tau217 performs better than p-tau181 as a biomarker of Alzheimer's disease.* Nat Commun, 2020. **11**(1): p. 1683.
11. Knopman, D.S. and J.S. Perlmutter, *Prescribing Aducanumab in the Face of Meager Efficacy and Real Risks.* Neurology, 2021. **97**(11): p. 545-547.
12. Budd Haeberlein, S., et al., *Two Randomized Phase 3 Studies of Aducanumab in Early Alzheimer's Disease.* J Prev Alzheimers Dis, 2022. **9**(2): p. 197-210.
13. Salloway, S., et al., *Amyloid-Related Imaging Abnormalities in 2 Phase 3 Studies Evaluating Aducanumab in Patients With Early Alzheimer Disease.* JAMA Neurol, 2022. **79**(1): p. 13-21.
14. van Dyck, C.H., et al., *Lecanemab in Early Alzheimer's Disease.* N Engl J Med, 2023. **388**(1): p. 9-21.
15. Lopez-Otin, C., et al., *The hallmarks of aging.* Cell, 2013. **153**(6): p. 1194-217.
16. Karch, C.M. and A.M. Goate, *Alzheimer's disease risk genes and mechanisms of disease pathogenesis.* Biol Psychiatry, 2015. **77**(1): p. 43-51.
17. Barnes, D.E. and K. Yaffe, *The projected effect of risk factor reduction on Alzheimer's disease prevalence.* Lancet Neurol, 2011. **10**(9): p. 819-28.

18. Silva, M.V.F., et al., *Alzheimer's disease: risk factors and potentially protective measures.* J Biomed Sci, 2019. **26**(1): p. 33.
19. Tosto, G., et al., *The Role of Cardiovascular Risk Factors and Stroke in Familial Alzheimer Disease.* JAMA Neurol, 2016. **73**(10): p. 1231-1237.
20. Satizabal, C.L., et al., *Incidence of Dementia over Three Decades in the Framingham Heart Study.* N Engl J Med, 2016. **374**(6): p. 523-32.
21. Rovelet-Lecrux, A., et al., *APP locus duplication causes autosomal dominant early-onset Alzheimer disease with cerebral amyloid angiopathy.* Nat Genet, 2006. **38**(1): p. 24-6.
22. Prasher, V.P., et al., *Molecular mapping of Alzheimer-type dementia in Down's syndrome.* Ann Neurol, 1998. **43**(3): p. 380-3.
23. Hashimoto, Y., et al., *Molecular characterization of neurohybrid cell death induced by Alzheimer's amyloid-beta peptides via p75NTR/PLAIDD.* J Neurochem, 2004. **90**(3): p. 549-58.
24. Kessels, H.W., et al., *The prion protein as a receptor for amyloid-beta.* Nature, 2010. **466**(7308): p. E3-4; discussion E4-5.
25. Wang, H.Y., et al., *Amyloid peptide Abeta(1-42) binds selectively and with picomolar affinity to alpha7 nicotinic acetylcholine receptors.* J Neurochem, 2000. **75**(3): p. 1155-61.
26. Wang, H.Y., et al., *Alpha 7 nicotinic acetylcholine receptors mediate beta-amyloid peptide-induced tau protein phosphorylation.* J Biol Chem, 2003. **278**(34): p. 31547-53.
27. Alberdi, E., et al., *Amyloid beta oligomers induce Ca2+ dysregulation and neuronal death through activation of ionotropic glutamate receptors.* Cell Calcium, 2010. **47**(3): p. 264-72.
28. Costa, R.O., et al., *Endoplasmic reticulum stress occurs downstream of GluN2B subunit of N-methyl-d-aspartate receptor in mature hippocampal cultures treated with amyloid-beta oligomers.* Aging Cell, 2012. **11**(5): p. 823-33.
29. Hardy, J.A. and G.A. Higgins, *Alzheimer's disease: the amyloid cascade hypothesis.* Science, 1992. **256**(5054): p. 184-5.
30. Hardy, J. and D. Allsop, *Amyloid deposition as the central event in the aetiology of Alzheimer's disease.* Trends Pharmacol Sci, 1991. **12**(10): p. 383-8.
31. Goedert, M., et al., *Multiple isoforms of human microtubule-associated protein tau: sequences and localization in neurofibrillary tangles of Alzheimer's disease.* Neuron, 1989. **3**(4): p. 519-26.
32. LoPresti, P., et al., *Functional implications for the microtubule-associated protein tau: localization in oligodendrocytes.* Proc Natl Acad Sci U S A, 1995. **92**(22): p. 10369-73.
33. Fischer, I. and P.W. Baas, *Resurrecting the Mysteries of Big Tau.* Trends Neurosci, 2020. **43**(7): p. 493-504.
34. Mukrasch, M.D., et al., *Structural polymorphism of 441-residue tau at single residue resolution.* PLoS Biol, 2009. **7**(2): p. e34.
35. Mylonas, E., et al., *Domain conformation of tau protein studied by solution small-angle X-ray scattering.* Biochemistry, 2008. **47**(39): p. 10345-53.
36. Jeganathan, S., et al., *Global hairpin folding of tau in solution.* Biochemistry, 2006. **45**(7): p. 2283-93.

37. Wischik, C.M., et al., *Isolation of a fragment of tau derived from the core of the paired helical filament of Alzheimer disease.* Proc Natl Acad Sci U S A, 1988. **85**(12): p. 4506-10.
38. Wegmann, S., et al., *The fuzzy coat of pathological human Tau fibrils is a two-layered polyelectrolyte brush.* Proceedings of the National Academy of Sciences of the United States of America, 2013. **110**(4): p. E313-E321.
39. von Bergen, M., et al., *Assembly of tau protein into Alzheimer paired helical filaments depends on a local sequence motif ((306)VQIVYK(311)) forming beta structure.* Proc Natl Acad Sci U S A, 2000. **97**(10): p. 5129-34.
40. Sawaya, M.R., et al., *Atomic structures of amyloid cross-beta spines reveal varied steric zippers.* Nature, 2007. **447**(7143): p. 453-7.
41. Khlistunova, I., et al., *Inducible expression of tau repeat domain in cell models of tauopathy - Aggregation is toxic to cells but can be reversed by inhibitor drugs.* Journal of Biological Chemistry, 2006. **281**(2): p. 1205-1214.
42. Goedert, M., et al., *Assembly of microtubule-associated protein tau into Alzheimer-like filaments induced by sulphated glycosaminoglycans.* Nature, 1996. **383**(6600): p. 550-3.
43. Kampers, T., et al., *RNA stimulates aggregation of microtubule-associated protein tau into Alzheimer-like paired helical filaments.* FEBS Lett, 1996. **399**(3): p. 344-9.
44. Wilson, D.M. and L.I. Binder, *Free fatty acids stimulate the polymerization of tau and amyloid beta peptides. In vitro evidence for a common effector of pathogenesis in Alzheimer's disease.* Am J Pathol, 1997. **150**(6): p. 2181-95.
45. Zhang, W., et al., *Heparin-induced tau filaments are polymorphic and differ from those in Alzheimer's and Pick's diseases.* Elife, 2019. **8**.
46. Chakraborty, P., et al., *Co-factor-free aggregation of tau into seeding-competent RNA-sequestering amyloid fibrils.* Nat Commun, 2021. **12**(1): p. 4231.
47. Schneider, A., et al., *Phosphorylation that detaches tau protein from microtubules (Ser262, Ser214) also protects it against aggregation into Alzheimer paired helical filaments.* Biochemistry, 1999. **38**(12): p. 3549-3558.
48. Despres, C., et al., *Identification of the Tau phosphorylation pattern that drives its aggregation.* Proc Natl Acad Sci U S A, 2017. **114**(34): p. 9080-9085.
49. Arendt, T., et al., *Reversible paired helical filament-like phosphorylation of tau is an adaptive process associated with neuronal plasticity in hibernating animals.* J Neurosci, 2003. **23**(18): p. 6972-81.
50. Arakhamia, T., et al., *Posttranslational Modifications Mediate the Structural Diversity of Tauopathy Strains.* Cell, 2020. **180**(4): p. 633-644 e12.
51. Quinn, J.P., et al., *Tau Proteolysis in the Pathogenesis of Tauopathies: Neurotoxic Fragments and Novel Biomarkers.* J Alzheimers Dis, 2018. **63**(1): p. 13-33.
52. Gu, J., et al., *Truncation of Tau selectively facilitates its pathological activities.* J Biol Chem, 2020. **295**(40): p. 13812-13828.
53. Li, L., et al., *Pathological Alterations of Tau in Alzheimer's Disease and 3xTg-AD Mouse Brains.* Mol Neurobiol, 2019. **56**(9): p. 6168-6183.

54. Zhang, Z., et al., *Cleavage of tau by asparagine endopeptidase mediates the neurofibrillary pathology in Alzheimer's disease.* Nat Med, 2014. **20**(11): p. 1254-62.
55. Kuchibhotla, K.V., et al., *Neurofibrillary tangle-bearing neurons are functionally integrated in cortical circuits in vivo.* Proc Natl Acad Sci U S A, 2014. **111**(1): p. 510-4.
56. Santacruz, K., et al., *Tau suppression in a neurodegenerative mouse model improves memory function.* Science, 2005. **309**(5733): p. 476-81.
57. Niewiadomska, G., et al., *Tau Oligomers Neurotoxicity.* Life (Basel), 2021. **11**(1).
58. Karran, E. and B. De Strooper, *The amyloid hypothesis in Alzheimer disease: new insights from new therapeutics.* Nat Rev Drug Discov, 2022. **21**(4): p. 306-318.
59. Congdon, E.E. and E.M. Sigurdsson, *Tau-targeting therapies for Alzheimer disease.* Nat Rev Neurol, 2018. **14**(7): p. 399-415.
60. Vogel, J.W., et al., *Four distinct trajectories of tau deposition identified in Alzheimer's disease.* Nat Med, 2021. **27**(5): p. 871-881.
61. Zempel, H. and E. Mandelkow, *Mechanisms of Axonal Sorting of Tau and Influence of the Axon Initial Segment on Tau Cell Polarity.* Adv Exp Med Biol, 2019. **1184**: p. 69-77.
62. Liu, C. and J. Gotz, *Profiling murine tau with 0N, 1N and 2N isoform-specific antibodies in brain and peripheral organs reveals distinct subcellular localization, with the 1N isoform being enriched in the nucleus.* PLoS One, 2013. **8**(12): p. e84849.
63. Candia, R.F., et al., *Importin-Mediated Pathological Tau Nuclear Translocation Causes Disruption of the Nuclear Lamina, TDP-43 Mislocalization and Cell Death.* Front Mol Neurosci, 2022. **15**: p. 888420.
64. Villasante, A., et al., *Binding of microtubule protein to DNA and chromatin: possibility of simultaneous linkage of microtubule to nucleic and assembly of the microtubule structure.* Nucleic Acids Res, 1981. **9**(4): p. 895-908.
65. Mansuroglu, Z., et al., *Loss of Tau protein affects the structure, transcription and repair of neuronal pericentromeric heterochromatin.* Sci Rep, 2016. **6**: p. 33047.
66. Violet, M., et al., *A major role for Tau in neuronal DNA and RNA protection in vivo under physiological and hyperthermic conditions.* Front Cell Neurosci, 2014. **8**: p. 84.
67. Loomis, P.A., et al., *Identification of nuclear tau isoforms in human neuroblastoma cells.* Proc Natl Acad Sci U S A, 1990. **87**(21): p. 8422-6.
68. Bou Samra, E., et al., *A role for Tau protein in maintaining ribosomal DNA stability and cytidine deaminase-deficient cell survival.* Nat Commun, 2017. **8**(1): p. 693.
69. Gunawardana, C.G., et al., *The Human Tau Interactome: Binding to the Ribonucleoproteome, and Impaired Binding of the Proline-to-Leucine Mutant at Position 301 (P301L) to Chaperones and the Proteasome.* Mol Cell Proteomics, 2015. **14**(11): p. 3000-14.
70. Montalbano, M., et al., *RNA-binding proteins Musashi and tau soluble aggregates initiate nuclear dysfunction.* Nat Commun, 2020. **11**(1): p. 4305.
71. Bridger, J.M., et al., *The nuclear lamina. Both a structural framework and a platform for genome organization.* FEBS J, 2007. **274**(6): p. 1354-61.

72. Coffinier, C., et al., *Abnormal development of the cerebral cortex and cerebellum in the setting of lamin B2 deficiency.* Proc Natl Acad Sci U S A, 2010. **107**(11): p. 5076-81.
73. Coffinier, C., et al., *Deficiencies in lamin B1 and lamin B2 cause neurodevelopmental defects and distinct nuclear shape abnormalities in neurons.* Mol Biol Cell, 2011. **22**(23): p. 4683-93.
74. Vergnes, L., et al., *Lamin B1 is required for mouse development and nuclear integrity.* Proc Natl Acad Sci U S A, 2004. **101**(28): p. 10428-33.
75. Jung, H.J., et al., *Regulation of prelamin A but not lamin C by miR-9, a brain-specific microRNA.* Proc Natl Acad Sci U S A, 2012. **109**(7): p. E423-31.
76. Nissan, X., et al., *Unique preservation of neural cells in Hutchinson- Gilford progeria syndrome is due to the expression of the neural-specific miR-9 microRNA.* Cell Rep, 2012. **2**(1): p. 1-9.
77. Mendez-Lopez, I., et al., *Hippocampal LMNA Gene Expression is Increased in Late-Stage Alzheimer's Disease.* Int J Mol Sci, 2019. **20**(4).
78. Prissette, M., et al., *Disruption of nuclear envelope integrity as a possible initiating event in tauopathies.* Cell Rep, 2022. **40**(8): p. 111249.
79. Keminer, O. and R. Peters, *Permeability of single nuclear pores.* Biophys J, 1999. **77**(1): p. 217-28.
80. Feldherr, C.M. and D. Akin, *The location of the transport gate in the nuclear pore complex.* J Cell Sci, 1997. **110 (Pt 24)**: p. 3065-70.
81. Sheffield, L.G., et al., *Nuclear pore complex proteins in Alzheimer disease.* J Neuropathol Exp Neurol, 2006. **65**(1): p. 45-54.
82. Lee, H.G., et al., *Aberrant localization of importin alpha1 in hippocampal neurons in Alzheimer disease.* Brain Res, 2006. **1124**(1): p. 1-4.
83. Eftekharzadeh, B., et al., *Tau Protein Disrupts Nucleocytoplasmic Transport in Alzheimer's Disease.* Neuron, 2018. **99**(5): p. 925-940 e7.
84. Paonessa, F., et al., *Microtubules Deform the Nuclear Membrane and Disrupt Nucleocytoplasmic Transport in Tau-Mediated Frontotemporal Dementia.* Cell Rep, 2019. **26**(3): p. 582-593 e5.
85. Ding, H., P.J. Dolan, and G.V. Johnson, *Histone deacetylase 6 interacts with the microtubule-associated protein tau.* J Neurochem, 2008. **106**(5): p. 2119-30.
86. Lipton, S.A., *Paradigm shift in neuroprotection by NMDA receptor blockade: memantine and beyond.* Nat Rev Drug Discov, 2006. **5**(2): p. 160-70.
87. Lithner, C.U., et al., *Disruption of neocortical histone H3 homeostasis by soluble Abeta: implications for Alzheimer's disease.* Neurobiol Aging, 2013. **34**(9): p. 2081-90.
88. Klein, H.U., et al., *Epigenome-wide study uncovers large-scale changes in histone acetylation driven by tau pathology in aging and Alzheimer's human brains.* Nat Neurosci, 2019. **22**(1): p. 37-46.
89. Nativio, R., et al., *An integrated multi-omics approach identifies epigenetic alterations associated with Alzheimer's disease.* Nat Genet, 2020. **52**(10): p. 1024-1035.
90. Frost, B., et al., *Tau promotes neurodegeneration through global chromatin relaxation.* Nat Neurosci, 2014. **17**(3): p. 357-66.

91. Sun, W., et al., *Pathogenic tau-induced piRNA depletion promotes neuronal death through transposable element dysregulation in neurodegenerative tauopathies.* Nat Neurosci, 2018. **21**(8): p. 1038-1048.
92. Zheng, Y., et al., *Inhibition of EHMT1/2 rescues synaptic and cognitive functions for Alzheimer's disease.* Brain, 2019. **142**(3): p. 787-807.
93. Lee, M.Y., et al., *Epigenome signatures landscaped by histone H3K9me3 are associated with the synaptic dysfunction in Alzheimer's disease.* Aging Cell, 2020. **19**(6): p. e13153.
94. Persico, G., et al., *Histone H3 Lysine 4 and 27 Trimethylation Landscape of Human Alzheimer's Disease.* Cells, 2022. **11**(4).
95. Morabito, S., et al., *Single-nucleus chromatin accessibility and transcriptomic characterization of Alzheimer's disease.* Nat Genet, 2021. **53**(8): p. 1143-1155.
96. Anderson, A.G., et al., *Single nucleus multiomics identifies ZEB1 and MAFB as candidate regulators of Alzheimer's disease-specific cis-regulatory elements.* Cell Genom, 2023. **3**(3): p. 100263.
97. Yamada, K., et al., *In vivo microdialysis reveals age-dependent decrease of brain interstitial fluid tau levels in P301S human tau transgenic mice.* J Neurosci, 2011. **31**(37): p. 13110-7.
98. Wang, Y., et al., *The release and trans-synaptic transmission of Tau via exosomes.* Mol Neurodegener, 2017. **12**(1): p. 5.
99. Pooler, A.M., et al., *Physiological release of endogenous tau is stimulated by neuronal activity.* EMBO Rep, 2013. **14**(4): p. 389-94.
100. Kaufman, S.K., et al., *Tau Prion Strains Dictate Patterns of Cell Pathology, Progression Rate, and Regional Vulnerability In Vivo.* Neuron, 2016. **92**(4): p. 796-812.
101. Clavaguera, F., et al., *Transmission and spreading of tauopathy in transgenic mouse brain.* Nat Cell Biol, 2009. **11**(7): p. 909-13.
102. Nussbaum, J.M., M.E. Seward, and G.S. Bloom, *Alzheimer disease: a tale of two prions.* Prion, 2013. **7**(1): p. 14-9.
103. Liu, G.H., et al., *Progressive degeneration of human neural stem cells caused by pathogenic LRRK2.* Nature, 2012. **491**(7425): p. 603-7.
104. Jiang, L., et al., *Interaction of tau with HNRNPA2B1 and N(6)-methyladenosine RNA mediates the progression of tauopathy.* Mol Cell, 2021. **81**(20): p. 4209-4227 e12.
105. Dawson, H.N., et al., *Inhibition of neuronal maturation in primary hippocampal neurons from tau deficient mice.* J Cell Sci, 2001. **114**(Pt 6): p. 1179-87.
106. Beaudoin, G.M., 3rd, et al., *Culturing pyramidal neurons from the early postnatal mouse hippocampus and cortex.* Nat Protoc, 2012. **7**(9): p. 1741-54.
107. Combs, B., et al., *Production of recombinant tau oligomers in vitro.* Methods Cell Biol, 2017. **141**: p. 45-64.
108. Norambuena, A., et al., *mTOR and neuronal cell cycle reentry: How impaired brain insulin signaling promotes Alzheimer's disease.* Alzheimers Dement, 2017. **13**(2): p. 152-167.
109. Raices, M. and M.A. D'Angelo, *Analysis of Nuclear Pore Complex Permeability in Mammalian Cells and Isolated Nuclei Using Fluorescent Dextrans.* Methods Mol Biol, 2022. **2502**: p. 69-80.

110. Livak, K.J. and T.D. Schmittgen, *Analysis of relative gene expression data using real-time quantitative PCR and the 2(-Delta Delta C(T)) Method.* Methods, 2001. **25**(4): p. 402-8.
111. Yoshiyama, Y., et al., *Synapse loss and microglial activation precede tangles in a P301S tauopathy mouse model.* Neuron, 2007. **53**(3): p. 337-51.
112. Wilcock, D.M., et al., *Progression of amyloid pathology to Alzheimer's disease pathology in an amyloid precursor protein transgenic mouse model by removal of nitric oxide synthase 2.* J Neurosci, 2008. **28**(7): p. 1537-45.
113. Underwood, R., et al., *14-3-3 mitigates alpha-synuclein aggregation and toxicity in the in vivo preformed fibril model.* Acta Neuropathol Commun, 2021. **9**(1): p. 13.
114. Brunello, C.A., et al., *Mechanisms of secretion and spreading of pathological tau protein.* Cell Mol Life Sci, 2020. **77**(9): p. 1721-1744.
115. Patterson, K.R., et al., *Characterization of prefibrillar Tau oligomers in vitro and in Alzheimer disease.* J Biol Chem, 2011. **286**(26): p. 23063-76.
116. Andorfer, C., et al., *Hyperphosphorylation and aggregation of tau in mice expressing normal human tau isoforms.* J Neurochem, 2003. **86**(3): p. 582-90.
117. Swanson, E., et al., *Extracellular Tau Oligomers Induce Invasion of Endogenous Tau into the Somatodendritic Compartment and Axonal Transport Dysfunction.* J Alzheimers Dis, 2017. **58**(3): p. 803-820.
118. Kelley, J.B., et al., *The defective nuclear lamina in Hutchinson-gilford progeria syndrome disrupts the nucleocytoplasmic Ran gradient and inhibits nuclear localization of Ubc9.* Mol Cell Biol, 2011. **31**(16): p. 3378-95.
119. Ferri, G., B. Storti, and R. Bizzarri, *Nucleocytoplasmic transport in cells with progerin-induced defective nuclear lamina.* Biophys Chem, 2017. **229**: p. 77-83.
120. Kelley, J.B. and B.M. Paschal, *Hyperosmotic stress signaling to the nucleus disrupts the Ran gradient and the production of RanGTP.* Mol Biol Cell, 2007. **18**(11): p. 4365-76.
121. Wu, J.W., et al., *Neuronal activity enhances tau propagation and tau pathology in vivo.* Nat Neurosci, 2016. **19**(8): p. 1085-92.
122. Ward, S.M., et al., *TOC1: characterization of a selective oligomeric tau antibody.* J Alzheimers Dis, 2013. **37**(3): p. 593-602.
123. Wang, Y. and E. Mandelkow, *Tau in physiology and pathology.* Nat Rev Neurosci, 2016. **17**(1): p. 5-21.
124. Sohn, C., et al., *Pathogenic tau decreases nuclear tension in cultured neurons.* Frontiers in Aging, 2023. **4**.
125. Rauch, J.N., et al., *LRP1 is a master regulator of tau uptake and spread.* Nature, 2020. **580**(7803): p. 381-385.
126. Fischer, A.H., *The diagnostic pathology of the nuclear envelope in human cancers.* Adv Exp Med Biol, 2014. **773**: p. 49-75.
127. Ahmed, M.S., et al., *Hutchinson-Gilford Progeria Syndrome: A Premature Aging Disease.* Mol Neurobiol, 2018. **55**(5): p. 4417-4427.
128. Oberdoerffer, P. and D.A. Sinclair, *The role of nuclear architecture in genomic instability and ageing.* Nat Rev Mol Cell Biol, 2007. **8**(9): p. 692-702.
129. Nakamura, M., et al., *Aberrant Accumulation of BRCA1 in Alzheimer Disease and Other Tauopathies.* J Neuropathol Exp Neurol, 2020. **79**(1): p. 22-33.

130. Dickson, J.R., et al., *Cytoplasmic Mislocalization of RNA Polymerase II Subunit RPB1 in Alzheimer Disease Is Linked to Pathologic Tau.* J Neuropathol Exp Neurol, 2021. **80**(6): p. 530-540.
131. Poleshko, A., et al., *H3K9me2 orchestrates inheritance of spatial positioning of peripheral heterochromatin through mitosis.* Elife, 2019. **8**.
132. Waldherr, S.M., et al., *Constitutive XBP-1s-mediated activation of the endoplasmic reticulum unfolded protein response protects against pathological tau.* Nat Commun, 2019. **10**(1): p. 4443.
133. Rauch, J.N., et al., *Tau Internalization is Regulated by 6-O Sulfation on Heparan Sulfate Proteoglycans (HSPGs).* Sci Rep, 2018. **8**(1): p. 6382.
134. Evans, L.D., et al., *Extracellular Monomeric and Aggregated Tau Efficiently Enter Human Neurons through Overlapping but Distinct Pathways.* Cell Rep, 2018. **22**(13): p. 3612-3624.
135. Wittmann, M., et al., *Synaptic activity induces dramatic changes in the geometry of the cell nucleus: interplay between nuclear structure, histone H3 phosphorylation, and nuclear calcium signaling.* J Neurosci, 2009. **29**(47): p. 14687-700.
136. Yang, Y., et al., *Improved calcium sensor GCaMP-X overcomes the calcium channel perturbations induced by the calmodulin in GCaMP.* Nat Commun, 2018. **9**(1): p. 1504.
137. Mahoney, R., et al., *Pathogenic Tau Causes a Toxic Depletion of Nuclear Calcium.* Cell Rep, 2020. **32**(2): p. 107900.
138. Liu, M., et al., *Chromatin tracing and multiplexed imaging of nucleome architectures (MINA) and RNAs in single mammalian cells and tissue.* Nat Protoc, 2021. **16**(5): p. 2667-2697.
139. Su, J.H., et al., *Genome-Scale Imaging of the 3D Organization and Transcriptional Activity of Chromatin.* Cell, 2020. **182**(6): p. 1641-1659 e26.